

RESEARCH

Open Access



# Hypoxemia exerts detrimental effects on the choroid plexuses and cerebrospinal fluid system in rats

Rawan Barakat<sup>1</sup>, Hameed Al-Sarraf<sup>1</sup> and Zoran Redzic<sup>1\*</sup>

## Abstract

**Background** Hypoxemia can cause secondary acute brain injury, but the mechanisms behind it are not entirely clear and could involve disturbances in the brain extracellular fluids. We aimed to explore the effects of hypoxemia on the choroid plexus (CPs) and cerebrospinal fluid (CSF) system in rats.

**Methods** Male Sprague Dawley rats were kept in O<sub>2</sub> control in vivo cabinet with either 21% (normoxia) or 8% O<sub>2</sub> (hypoxemia) for up to 48 h. In some cases, signaling of selected cytokines was inhibited prior to hypoxemia. CSF and blood samples were collected by *Cisterna Magna* puncture and through venous catheters, respectively. The percentages of dead cells in the CPs and ependymal layers (EL) after hypoxemia or normoxia was estimated using TUNEL staining. CP's ultrastructure was analyzed by transmission electron microscopy. Protein concentration in the CSF and plasma was measured and the CSF albumin-to-total protein ratios were estimated. Concentrations of hypoxia-related cytokines in the CSF and plasma samples were estimated using the multiplex immunoassay. Data was analyzed by one-way ANOVA followed by either Bonferroni or Tukey's multiple comparison tests, or Student's t-test. Results are presented as mean  $\pm$  SD;  $p < 0.05$  was considered statistically significant.

**Results** Duration of hypoxemia exerted significant effects on the cell viability in the CPs ( $p < 0.01$ ) and EL ( $p < 0.01$ ) and caused apoptosis-related changes in the CP. Hypoxemia had significant effects on the protein concentration in the CSF ( $p < 0.05$ ), but not in plasma ( $p > 0.05$ ), with a significant increase in the CSF albumin-to-total protein ratio after 6 h hypoxemia ( $p < 0.05$ ). Thirty-two cytokines were detected in the CSF. Hypoxemia caused a statistically significant reduction in the concentrations of 12 cytokines, while concentrations of erythropoietin (EPO) and vascular endothelial growth factor (VEGF) increased significantly. Exposure to hypoxemia after inhibitions of EPO, VEGF, or tumor necrosis factor alpha (TNF $\alpha$ ) signaling resulted in more dead cells ( $p < 0.01$ ), less dead cells ( $p < 0.01$ ) and more dead cells ( $p < 0.01$ ) in the CPs, respectively, when compared to the number of dead cells when these cytokines were not inhibited. The density of macrophages in the CPs decreased significantly during hypoxemia; that effect was cancelled out by TNF $\alpha$  inhibition.

**Conclusion** Hypoxemia had detrimental effects on the CPs and CSF system, which was modulated by hypoxia- and inflammation-related cytokines.

**Keywords** Isobaric hypoxemia, Hypoxia, Cerebrospinal fluid, Extracellular fluid, Cell death, Choroid plexus, Cytokines, Macrophages

\*Correspondence:

Zoran Redzic  
zoran.redzic@ku.edu.kw

<sup>1</sup> Department of Physiology, College of Medicine, Kuwait University, P.O. Box 24923, 13110 Safat, Kuwait



© The Author(s) 2025. **Open Access** This article is licensed under a Creative Commons Attribution-NonCommercial-NoDerivatives 4.0 International License, which permits any non-commercial use, sharing, distribution and reproduction in any medium or format, as long as you give appropriate credit to the original author(s) and the source, provide a link to the Creative Commons licence, and indicate if you modified the licensed material. You do not have permission under this licence to share adapted material derived from this article or parts of it. The images or other third party material in this article are included in the article's Creative Commons licence, unless indicated otherwise in a credit line to the material. If material is not included in the article's Creative Commons licence and your intended use is not permitted by statutory regulation or exceeds the permitted use, you will need to obtain permission directly from the copyright holder. To view a copy of this licence, visit <http://creativecommons.org/licenses/by-nc-nd/4.0/>.

## Background

Normal partial pressure of O<sub>2</sub> in the arterial blood (PaO<sub>2</sub>) is above 95 mmHg and this is essential for sufficient supply of O<sub>2</sub> to the tissues. To maintain PaO<sub>2</sub> at this value, normal partial pressure of inspired oxygen (PiO<sub>2</sub>, normally 160 mmHg) and preserved lung function are essential. When either of these two are affected, PaO<sub>2</sub> decreases. Hypoxemia is a condition in which PaO<sub>2</sub> is lower than 90 mmHg and it may or may not cause tissue hypoxia, which depends on the severity of hypoxemia and on metabolic demands [1]. Severe hypoxemia usually occurs due to a lung injury (also known as type 1 respiratory failure (T1RF)) or at a very high altitude, where PiO<sub>2</sub> is low. T1RF can cause secondary acute brain injury (sABI), which can cause neurological symptoms ranging from a mild to severe cognitive deficits [2, 3]. Severe T1RF is commonly associated with acute lung injury and developed in 16–40% of patients that were admitted to hospitals due to Severe Acute Respiratory Syndrome Coronavirus 2 (SARS-CoV-2) infection [4]. In those who recover, a disturbance in cognitive functions is frequently observed [5]. A study revealed that these disturbances were present in 75–100, 30 and 25% of patients at discharge, after 1 year and after 6 years, respectively [6]. In those who did not recover, postmortem analysis revealed loss of neurons in the cerebral cortex, hippocampus, and Purkinje cell layer [7].

Precise mechanisms that link hypoxemia to sABI are not clear. Though hypoxic injury during severe hypoxemia as a cause of sABI is not disputable [7], it is probably not the only mechanism involved. This is because partial pressure of oxygen in the cerebral cortex (PtO<sub>2</sub>) of rats exposed to conditions that lowered PaO<sub>2</sub> to levels seen in severe T1RF was around 6 mmHg [8], which was well above the threshold of ≤ 1 mmHg at which activity of the Complex 4 in mitochondria gets impeded [9]. Yet, cell death in the cerebral cortex of those rats was confirmed.

Several other mechanisms could also contribute to sABI. Brain homeostasis largely relies on the constant composition and flow of the brain extracellular fluids (ECFs), which are interstitial fluid (ISF) and cerebrospinal fluid (CSF) [10]. CSF is constantly produced, more than 50% by the choroid plexuses (CPs) [11] and the remaining amount being derived from the brain ISF and secreted by the ependymal layer (EL) that lines the cerebral ventricles [12]. CPs are complex networks of capillaries covered by the modified ependymal epithelium that is the site of the blood-cerebrospinal fluid barrier (BCSFB), which plays an essential role in maintaining constant composition of the brain ECFs [11]. CSF is an important source of the brain ISF by a constant slow bulk flow of the CSF through the Virchow-Robin spaces into the ISF, which is then in turn partially drained back

into the CSF [13]. About 5–10% CSF diffuses into the ISF of the subventricular zones across the ependymal lining (EL) of the ventricles. CSF-borne peptides, which could be either produced by the CPs [14] or by various brain cells, can reach distant neurons, including neuronal stem cells [15]. Damage to the CPs can cause an increase in the permeability of the BCSFB, while injury to the CPs and EL can alter the production and flow of the brain ECFs.

Focal ischemic hypoxia of the CPs occurs rarely [16], while a temporary ischemic hypoxia of the CPs due to a global hypoperfusion, which occurs more frequently, caused increased expression of advanced glycation end-product receptors in the CP epithelial cells [17]. Animal studies that used 30 min transient common carotid artery occlusion in rats found ischemic necrosis in the CP that occurred earlier than in the hippocampus [18] which indicated selective vulnerability of these structures to ischemic hypoxia. CPs are also known to be sensitive to perinatal hypoxia [19, 20] and they could suffer damage during ischemic stroke caused by middle cerebral artery occlusion [21].

However, hypoxemia by its nature largely differs from ischemia. Though hypoxemia can cause hypoxia, the blood flow is preserved, and thus tissues can get glucose and pyruvate that could be used for ATP production by glycolysis. Yet, no data exist if hypoxemia can cause damage CP/CSF system.

Another mechanism that could link hypoxemia to sABI could be inflammation, since activated microglia can phagocytose neurons and/or release reactive oxygen species that can induce neuronal cell death [22]. Hypoxemia can trigger tissue injury-related and tissue injury-unrelated inflammation. Hypoxic cell death in the CPs or in the brain is recognized by stromal macrophages of the CPs and brain microglia, respectively, which causes activation of innate immune responses leading to the production of proinflammatory cytokines and the activation of adaptive immunity to clear up dead cells. Tissue hypoxia also triggers inflammatory processes mediated by prolyl hydroxylase domain (PHD) -mediated activation nuclear factor kappa-light-chain-enhancer of activated B cells (NF-κB) pathway [23, 24], which is irrespective of tissue injury and contributes to macrophages/microglia activation and cytokine secretion in the ECFs. The CSF can be sampled relatively easily when compared to the brain ISF, so patterns of changes in concentrations of cytokines could be valuable to assess if inflammatory events take place in the brain. It has been shown earlier that high-altitude hypoxemia caused leukocytosis in the brain [25] and elevated levels of several hypoxia- and inflammation-related cytokines in the CSF [2, 25]. However, existing studies described concentrations of only

few cytokines, which does not provide a comprehensive picture of events during hypoxemia.

In this study we induced hypoxemia in the rats by reducing  $PiO_2$ . This hypoxemia was by its severity similar to T1RF-associated hypoxemia in humans. We revealed that these conditions were detrimental for CP epithelial cells and ELs and that these effects were modulated by hypoxia-related cytokines. We detected 32 hypoxia- and inflammation-related cytokines in the CSF, but the pattern of changes in their concentrations did not suggest that hypoxemia caused inflammation in the brain.

## Material and methods

### Animals

A total of 54 Sprague Dawley male rats were used, which were bred in the Animal Resource Centre (ARC), Kuwait University and kept in 50% humidity, with a 12 h/12 h day/dark cycle and access to food and water ad libitum. The rats were 10–12 weeks old with body weight 240–280 g and could therefore be considered young adults [26]. The rationale behind the decision to conduct the study exclusively on male rats was based on previous studies that reported a gender difference in rats and humans in responses to hypoxia/ischemia [27–29] and in the mechanism of hypoxic cell death [30]. All procedures in the rats were conducted following the guidelines of laboratory animal care at Kuwait University, and the Institutional Animal Ethics Committee of Health Sciences Center approved all experimental protocols, which comply with the National Research Council's Guide for the care and use of laboratory animals.

### Anesthesia and pain alleviation

For the recovery anesthesia, rats were anesthetized with ketamine (60 mg/kg)/xylazine (10 mg/kg) intramuscularly. For terminal anesthesia, urethane, 1.2 g/kg intraperitoneally (i.p.) was used. During the recovery period after the surgery (e.g., implantation intracerebroventricular cannula) for the following 3 days the rats received

Tramadol (0.1 mg/kg s.c.) to alleviate pain and Enrofloxacin (0.05 mg/kg s.c.) once a day to prevent infection.

### Isobaric hypoxemia

Details of the protocol have been published already [8]. Briefly, rats were placed in  $O_2$  control in vivo cabinet (Coy Laboratories, USA), which was equipped with advanced controller and sensors to precisely monitor  $O_2$  levels. They were exposed either to 21%  $O_2$  (normoxia) or to 8%  $O_2$  (hypoxemia) for up to 48 h, the latter one being sometimes followed by 24 h normoxia (recovery) (Fig. 1A). Percentage of  $CO_2$  was recorded and maintained at  $<0.5\%$ .

### Experimental design and timeline of sample collections

The experimental design is summarized in the diagram below (Fig. 1B), which shows how three sets of rats were used to collect samples:

1. Set no 1 was used to collect brain samples for assessment of cells death and number of macrophages and for CSF collection. After periods of normoxia, hypoxemia, or recovery, rats were terminally anesthetized and CSF samples were collected by a puncture of *Cisterna Magna* as previously explained (see below) and were used to measure concentrations of cytokines. At the end of the experiment's brains were fixed and sliced to assess cell death in the CPs and ELs, and the number of macrophages in the CPs.
2. Set no 2 was used to study effects of inhibition of cytokines' signaling on cell death. Inhibitions of signaling of erythropoietin (EPO), vascular endothelial growth factor (VEGF), and tumor necrosis factor-alpha ( $TNF\alpha$ ) was done prior to the experiments explained above.
3. Set no 3 was used for collection of CPs and plasma samples. Blood samples were collected by jugular

(See figure on next page.)

**Fig. 1** Summary of the isobaric hypoxemia model and experimental design. Image **A**. Rats were placed in the cabinet in a custom-made metabolic-style cage. The  $O_2$  sensor plugged in the cabinet was connected to the  $O_2$  controller to regulate the percentage of  $O_2$  in  $N_2$ .  $CO_2$  was monitored using a gas analyzer and a scrubbing system was used to maintain it  $<0.5\%$ . Image **B**. The experiments were divided into 3 sets: (1) CSF and brain samples were collected after normoxia (0 h), 24 h, 48 h hypoxemia, and 24 h recovery after hypoxemia. Brains were fixed and sliced to assess CP and EL cell viability, and macrophages numbers. (2) Inhibition experiments for EPO, VEGF, and  $TNF\alpha$  signaling were conducted, with brains fixed during normoxia and after hypoxemia to examine cell viability. The macrophages numbers were further assessed after inhibiting  $TNF\alpha$  signaling. EPO inhibitor was injected ICV, while VEGF, and  $TNF\alpha$  inhibitor were injected i.p. (3) Jugular veins were catheterized (left side schematic) to collect blood samples at various hypoxemia time points. Prior to the experiment, the catheter was connected to an external needle through tubing filled with heparinized saline (right side schematic), allowing for frequent blood sampling without opening the  $O_2$  control cabinet. Due to clotting of the catheters after repetitive sampling, in one set of animals blood samples were collected during normoxia and after 2 and 6 h hypoxemia and in another set of animals during normoxia and after 24 and 48 h hypoxemia. CPs were collected to test the CPs ultrastructure by transmission electron microscopy after normoxia and 48 h hypoxemia. The schematic diagrams were created using BioRender.com



vein catheterization (Fig. 1B) that was performed as described earlier [31]. At the end of experiments, rats were terminally anesthetized, and CPs were collected from the lateral ventricle for Transmission electron microscopy (TEM) analysis.

### Collection of the CSF samples

Collection of the CSF samples was done as previously explained [32]. Briefly, rats were anesthetized, and a small rostro-caudal incision made in the neck region. A blunt dissection of the neck muscles along the midline was performed until the atlanto-occipital membrane was exposed. The head of the animal was maintained at around 45° from horizontal. Then, a pulled sharp glass micropipette with a long tip was inserted into the *Cisterna magna* at 30° from horizontal by a puncture through the membrane and through the underlying *dura mater*. Once the tip of the micropipette was in the *Cisterna magna*, a slow flow of the clear, spring water-like fluid (i.e., CSF) into the pipette tip could be seen. If a trace of red color was observed in the sample at this point, further collection was abandoned, and the sample was discarded. Then, a slight suction was applied that caused further flow of the CSF to the glass pipette, allowing collection of 40–80 µL samples. The collected sample was checked again against the white background and against a diffuse light, which are standard techniques to check for blood contamination of the CSF samples [33].

### Transmission electron microscopy

Rats were terminally anesthetized, and the brains were perfused with saline then 4% paraformaldehyde in phosphate buffer solution (PBS) via the heart. The CPs were dissected from the brain, transferred to 3% glutaraldehyde overnight and post fixed in 1% Osmium tetroxide. The sample was then dehydrated through an alcohol series and embedded in epoxy resin. Following polymerization, 100 nm thin sections were double stained and analyzed using JEM-1200 EX II 120 kV TEM (JEOL, Japan). This was a descriptive (qualitative), rather than quantitative analysis. We analyzed a total of 4 choroid plexuses collected from each group (control rats and rats after hypoxemia). We randomly selected two regions in each plexus for analysis. Selected images were described by a protocol-blind expert.

### Cell death in the choroid plexuses and ependyma layers

Assessment of number of dead cells in the CPs and EL was done using TUNEL staining, which detects cell death-associated DNA fragmentation (3'-OH DNA termini). At the end of the experiments, the brains were perfused with 100 ml saline through the heart for then with

4% paraformaldehyde in PBS for fixation. The fixed brains were then embedded in paraffin wax (Paraplast X-TRA, Sigma Aldrich). Paraffin blocks were prepared using the TES Valida Paraffin Embedding Center (MEDITE, Germany). The brains were sliced into 5 µm sections, mounted on glass slides, and dried on a hot plate at 37 °C overnight. The staining protocol consisted of deparaffinization, antigen retrieval, and TUNEL reaction mixture addition. For antigen retrieval, slides were immersed in boiling 2.94 g/L Na-citrate (pH 6) for 3–5 min, then washed with PBS. The sections were incubated in the TUNEL reaction mixture for 75 min, washed with PBS, and then incubated with 4',6-diamidino-2-phenylindole (DAPI) for 10 min to stain cell nuclei. After a final wash, sections were mounted with DPX medium and covered with cover slips. Positive and negative control images are provided in supplementary Fig. 1.

The images were captured using a ZEISS LSM 980 m microscope (Zeiss, Germany). The total numbers of DAPI-positive and TUNEL-positive cells were counted using the ComDet plugin version 0.5.5 of the FIJI image processing package (Image J software, (NIH, USA); a guided plugin that identifies and counts cells within an image by setting specific parameters, including particle size (in pixels) and intensity threshold. Manual counting was performed occasionally on random images by ZEN 3.5 software (Zeiss, Germany) to confirm the accuracy of the cell counting protocol, the accuracy of the cell counting protocol was above 97%.

One randomly selected slide was used per rat. Three images from 3 different regions of CPs or EL in the lateral ventricles were captured from each slide. The percentage of TUNEL-positive, indicating cell death, was assessed in relation to the total DAPI-positive cells (nuclei) for each individual image. The average percentage of cell death in a sample was calculated from the 3 images taken per slide, and the overall average of these samples was used for statistical analysis.

### Detection of ionized calcium binding adaptor molecule-1 (Iba1)-positive cells in the CPs

After antigen retrieval, the brain slides were incubated overnight with Polyclonal Rabbit Anti Iba1 antibody (Fujifilm Wako, Japan), 1/500 in phosphate buffer solution (PBS) containing 1% bovine serum albumin (BSA) and Triton- $\times$ 100, which was followed by incubation with secondary, Anti-rabbit IgG antibody that was conjugated to Alexa Fluor 488 (Invitrogen, US), 1/500 in PBS containing 1% BSA and Triton- $\times$ 100. One randomly selected slide was used per rat and 5 images from different regions of the CPs were taken from each slide. Images were captured using confocal microscope LSM 900 m microscope (Zeiss, Germany) at 20X magnification. The cell counting

was done using ComDet plugin version 0.5.5 of the FIJI image processing package (Image J software, (NIH, USA). CPs were usually located only in a part of the slide; for that reason, the region of interest (ROI) was selected manually in the software (Supplementary Fig. 3) and the macrophage densities were calculated as number of Iba-1 positive cells in the ROI divided by the surface area of the ROI. Manual counting of the Iba-1 positive cells was performed occasionally on random images by ZEN 3.5 software (Zeiss, Germany) to confirm the accuracy of the cell counting protocol, which was above 99.8%.

#### Estimation of protein concentration in the CSF and plasma

Protein concentration was estimated by measuring the UV absorbance at 280 nm. Briefly, 2  $\mu$ L of CSF or plasma samples in duplicates or PBS (blanks) were placed in the micro volume plate and absorbance at 280 nm was estimated by BioTek Epoch 2 Spectrophotometer (Agilent Technologies, US). Protein concentration was estimated by Gen6 software using the Beer-Lambert law.

#### Separation of proteins by gel electrophoresis

Separation of proteins was based on their size, using SDS-PAGE. All samples were boiled at 95 °C for 5 min and then centrifuged at 16,000 $\times$ g for 5 min. Volumes of the samples were adjusted to load a total of 6.65  $\mu$ g protein/sample, which was added to the homogenization buffer and 4 $\times$ loading dye. Protein concentration was estimated as explained above. Stain-free gradient polyacrylamide gels (4–20%, Bio-Rad, USA) were used for electrophoresis, which was run at 200 V for 30 min. Following electrophoresis, gel activation was performed by exposing the stain-free gel matrix to UV light in the ChemiDoc MP imaging system. This UV exposure activates the trihalo compound in the gel, causing it to crosslink with tryptophan residues in the proteins and produce a fluorescent signal. Images were captured using the ChemiDoc imaging hardware.

#### Concentrations of cytokines in the CSF and plasma samples

Concentrations of cytokines in the CSF and plasma samples were estimated using Merck Millipore Milliplex magnetic bead panels-Multiplex assay, according to the manufacturer instructions (MILLIPLEX<sup>®</sup> Multiplex Assays, MERCK, USA). The fluorescence in the wells was read using Luminex<sup>®</sup> 200TM hardware with xPONENT<sup>®</sup> Software. The cytokine concentrations were estimated in duplicates and the mean of the two values was used for analysis. The list of cytokines that were estimated is presented in Supplementary Table 1. For some cytokines, mean fluorescence intensity (MFI) values were within the concentration ranges in the standards, so the concentrations (g/L) could be determined. For other cytokines,

MFI value(s) were, at least in one sample, out of the range of the standard curve(s). Thus, according to the manufacturer guidelines, we presented amounts of such cytokines as MFIs. Since the lowest limits of the standard curves were largely different between various cytokines (e.g., from 0.6 to 110 pg/ml), the fact that concentration of a cytokine was expressed as MFI did not imply that its concentrations was lower than concentrations of cytokines that had concentrations expressed as pg/ml. We also estimated the CSF/plasma ratio for each of these cytokines by dividing concentration of a cytokine in the CSF to its concentration in the plasma.

The concentrations of cytokines were analyzed to estimate the effect of duration of hypoxia on cytokines' concentration as well as the concentration changes for every cytokine between each time point. We also calculated the fold change, which is the ratio of the mean concentration of a cytokine in each time point of hypoxemia to that during normoxia. This is because several microarray studies emphasized the importance of the fold change analysis in drawing conclusions about their concentrations / expressions changes [34–36]. This approach offers evaluation of the data that is often more meaningful from the physiological point of view than a statistical analysis only [34].

#### Inhibition of cytokine signaling during hypoxemia

We identified increase in concentrations of three cytokines in the ECFs of the brain during hypoxemia: EPO and VEGF increased in the CSF and TNF $\alpha$  increased in the brain ISF (the data not shown for the latter one). To assess their role in hypoxemia-induced cell death, we first inhibited their signaling and then subjected rats to hypoxemia. The following protocols were applied:

**EPO inhibition.** We used recombinant EPO soluble receptor (sEPOR) (Sigma Aldrich, Germany) that binds EPO with high affinity. This glycosylated recombinant protein has MW of 36 KDa and it is water soluble, however, to the best of our knowledge, there is no data on pharmacokinetics of this molecule after systemic application. Its water solubility implies that after intracerebroventricular (ICV) injection it gets freely distributed in the CSF, so the CSF gets largely depleted of free EPO, which implies that EPO signaling on both CP epithelium and ependymal layer was affected by this protocol. To inject sEPOR in the lateral ventricle, we implanted a cannula in the left lateral ventricle using the following coordinates: anteroposterior – 1.08 mm, mediolateral+1.6 mm from the Bregma, and dorsoventrally – 4.3 mm from the surface of the skull. After 3 days recovery, we injected ICV either a bolus of 7  $\mu$ L PBS with 0.1% BSA that contained 8  $\mu$ g of sEPOR or the vehicle (Supplementary Fig. 2). Twenty minutes after the injection, the rats were subjected to hypoxemia for 48 h.

**VEGF inhibition.** Axitinib inhibits VEGF receptors 1–3 with  $IC_{50} < 1$  nM and easily crosses the blood brain barrier in rats [37]. It gets rapidly absorbed in humans with a median plasma  $T_{max}$  of 2.2 h after oral application [38], which is followed by rapid metabolism and clearance with  $T_{1/2}$  in plasma 10.6 h and a rapid decline in plasma concentrations after 24 h to  $< 10\%$  of the  $C_{max}$  [38]. For this reason, we injected i.p. either 1 ml of PBS containing 6.5% DMSO with 8.3 mg/Kg of Axitinib (Pfizer, USA) or the vehicle and exposed animals to hypoxemia 20 min after the injections. Due to the above-mentioned pharmacokinetic properties, it would be required to repeat the administration after 24 h. To avoid opening of the cabinet, hypoxemia in this group was limited to 24 h.

**TNF inhibition.** We used etanercept, which is a soluble recombinant tumor necrosis factor receptor fusion protein [39], to bind soluble TNF $\alpha$  and thus, inhibits its action on the CP epithelium. Intraperitoneal (i.p.) and subcutaneous applications of this protein are commonly used in rats [40, 41], which were followed by a slow absorption and half-life in plasma in rats longer than 2 days [42]. We applied i.p. injections of either a bolus of saline that contained 5.7 mg/kg of Etanercept (IchorBio, USA) or the vehicle. After 20 min, the animals were exposed to 48 h hypoxemia. Since this complex does not pass the blood–brain barrier [43], this protocol lowered the concentration of TNF $\alpha$  peripherally.

### Statistical analysis

The data are presented as raw data and means  $\pm$  SDs in the figures and means  $\pm$  SDs in the text. One way ANOVA with Bonferroni test for multiple comparisons was used to assess effect of hypoxemia on the number of dead cells in the CPs and ELs in various groups and to compare densities of Iba1-positive cells in the CPs after normoxia, hypoxemia, and hypoxemia with etanercept application. Concentration of cytokines in CSF and plasma samples at various time points were assessed using Mixed-Measures ANOVA. The total protein concentrations in CSF and plasma, and the CSF albumin band density/total CSF protein bands densities ratio were analyzed by one-way ANOVA with Tukey test for

multiple comparisons. Student t-test for independent samples was used to compare the number of TUNEL-positive cells after hypoxemia with or without cytokines' inhibitors. Normality of data distribution was analyzed with Shapiro–Wilk's  $W$  test and homogeneity of variance with Levene's test. Statistical significance for all tests was set at  $p < 0.05$ . Statistical analyses were done in TIBCO Statistica v. 13.3 software and GraphPad Prism 9 software.

## Results

### Effects of hypoxemia on cell death in the CPs and EL

The duration of hypoxemia had a significant effect on cell viabilities in the CPs ( $F(3,17) = 9.57$ ,  $p < 0.01$ , Fig. 1A, B) and in the EL ( $F(3,17) = 37.56$ ,  $p < 0.01$ , Fig. 2C, D). After 24 h and 48 h hypoxemia,  $21.43 \pm 4.59\%$  and  $32.26 \pm 7.21\%$  in CPs, and  $24 \pm 8.23\%$  and  $29 \pm 8\%$  in ELs were TUNEL positive, respectively ( $n = 5$ /group). The percentages of TUNEL positive cells in CPs after 24 h hypoxemia did not differ significantly from the percentages in normoxia group, which means that the CP cells were resilient to hypoxemia during this period. However, after 48 h hypoxemia and recovery the percentages of TUNEL positive cells were significantly higher when compared to normoxia ( $p < 0.05$ , Fig. 2B). The percentages of TUNEL positive cells in the EL were significantly higher than in normoxia at all time points ( $p < 0.05$ , Fig. 2D), which indicated that this cell layer is sensitive to hypoxemia. No further significant increase in the percentage of TUNEL positive cells was observed in the CPs during the recovery ( $30.23 \pm 6.89\%$ ,  $n = 5$ ,  $p > 0.05$ , Fig. 2C) when compared to 48 h hypoxemia, while the percentage of TUNEL positive cells in ELs almost doubled during the recovery ( $59.61 \pm 12.00\%$ ,  $p < 0.01$  vs. 48 and 24 h hypoxemia, Fig. 2D). There was a relatively high percentage of TUNEL-positive cells observed in the CPs and ELs after normoxic conditions, which was probably caused by cell death during the brain fixation protocol.

(See figure on next page.)

**Fig. 2** Cell death in the CP and EL during normoxia and after hypoxemia. Pannels **A** and **C** images **A–D** are typical images obtained for CP (2A) and EL (2C) after normoxia, 24 h hypoxemia, 48 h hypoxemia and 48 h hypoxemia followed by 24 h recovery, respectively. The nuclei are stained with DAPI (blue) and dead cells are identified as TUNEL-positive (green). The bar is 50  $\mu$ m. Arrows in 2C indicate EL. **B** and **D**. The graphs represent the graphs represent raw data in each group and the mean  $\pm$  SD in CPs (2B) and ELs (2D) during normoxia (N,  $n = 6$ ); 24 h hypoxemia (H24,  $n = 5$ ), 48 h hypoxemia (H48,  $n = 5$ ) and 24 h hypoxemia followed by the recovery (H48 + N24,  $n = 5$ ). Shapiro–Wilk's test for normality and Levene's test for homogeneity of variance were not significant ( $p > 0.05$ ). The duration of hypoxemia showed a significant increase in cell death in both CPs and EL ( $P < 0.01$ ). Bonferroni test was used for multiple comparisons between the groups. Signs indicate: \*— $p < 0.05$  N vs. other groups, #— $p < 0.05$  H48 + N24 vs. H24 and H48. **E** and **F**. TEM morphology of the CP epithelium after normoxia (1E) and hypoxemia (1F). The bar is 1  $\mu$ m. Solid black arrows—microvilli; solid white arrows—mitochondria; dashed white arrow—nucleolus; dashed red arrow—chromatin; dashed yellow arrows—vacuoles

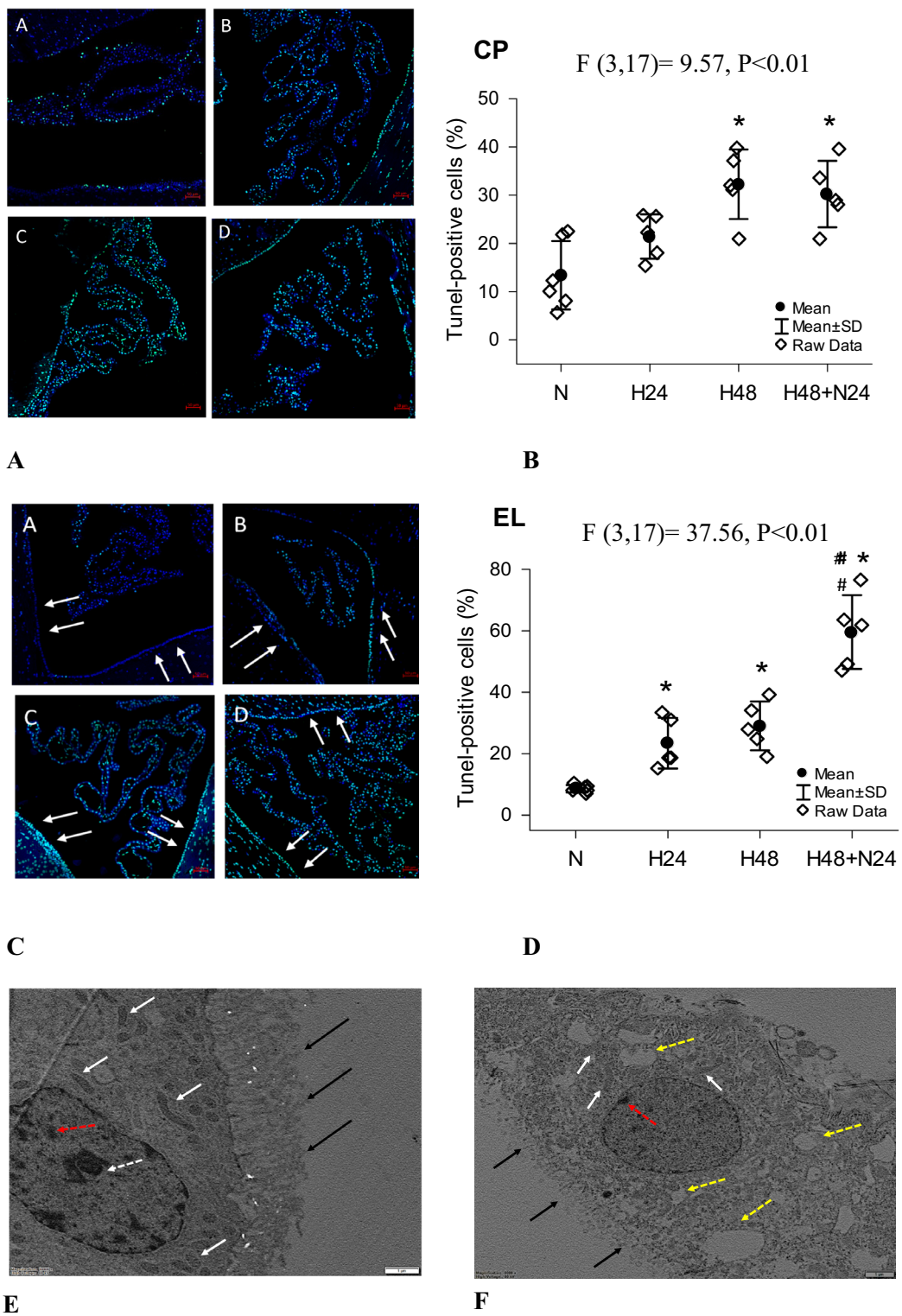


**Fig. 2** (See legend on previous page.)

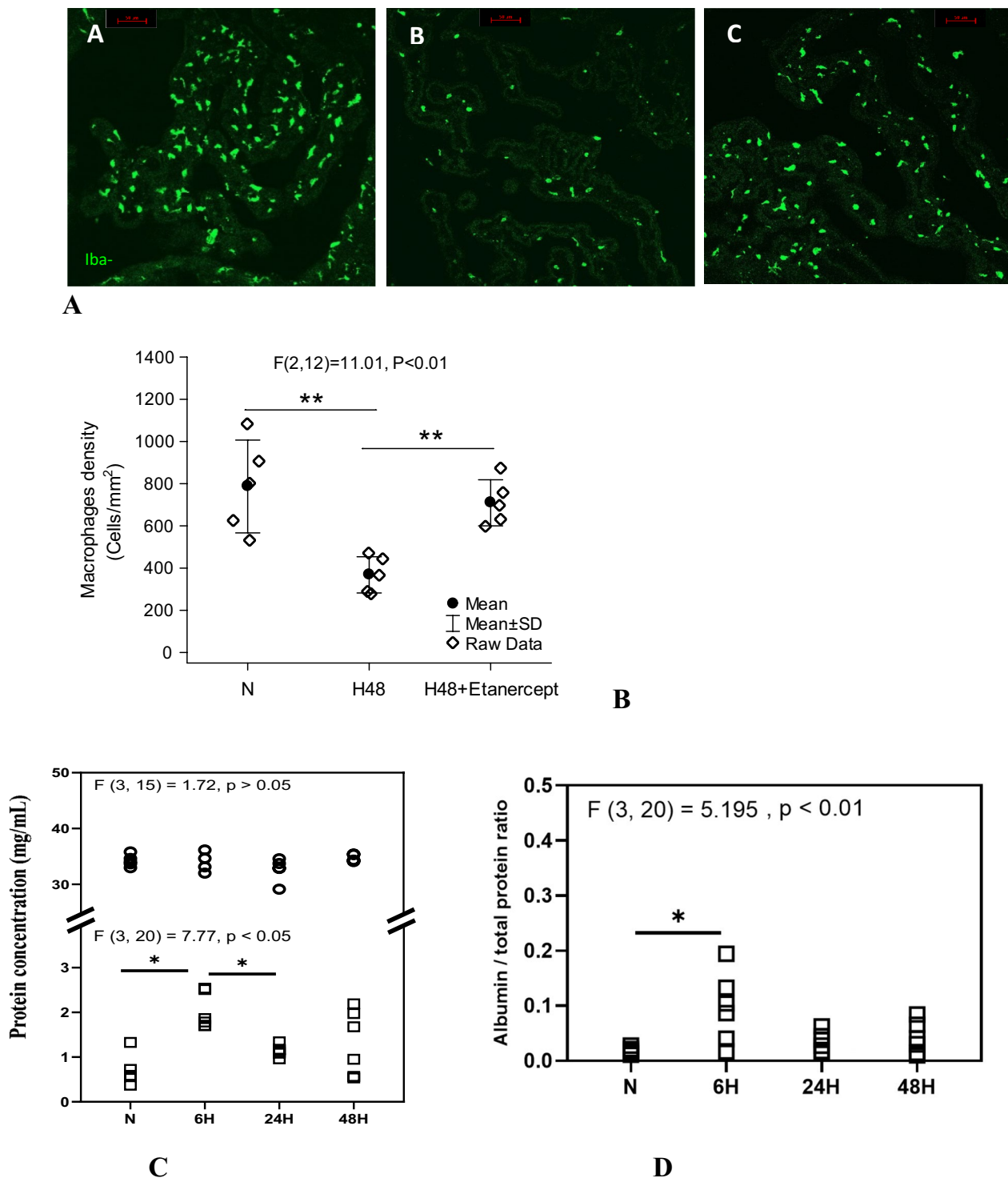
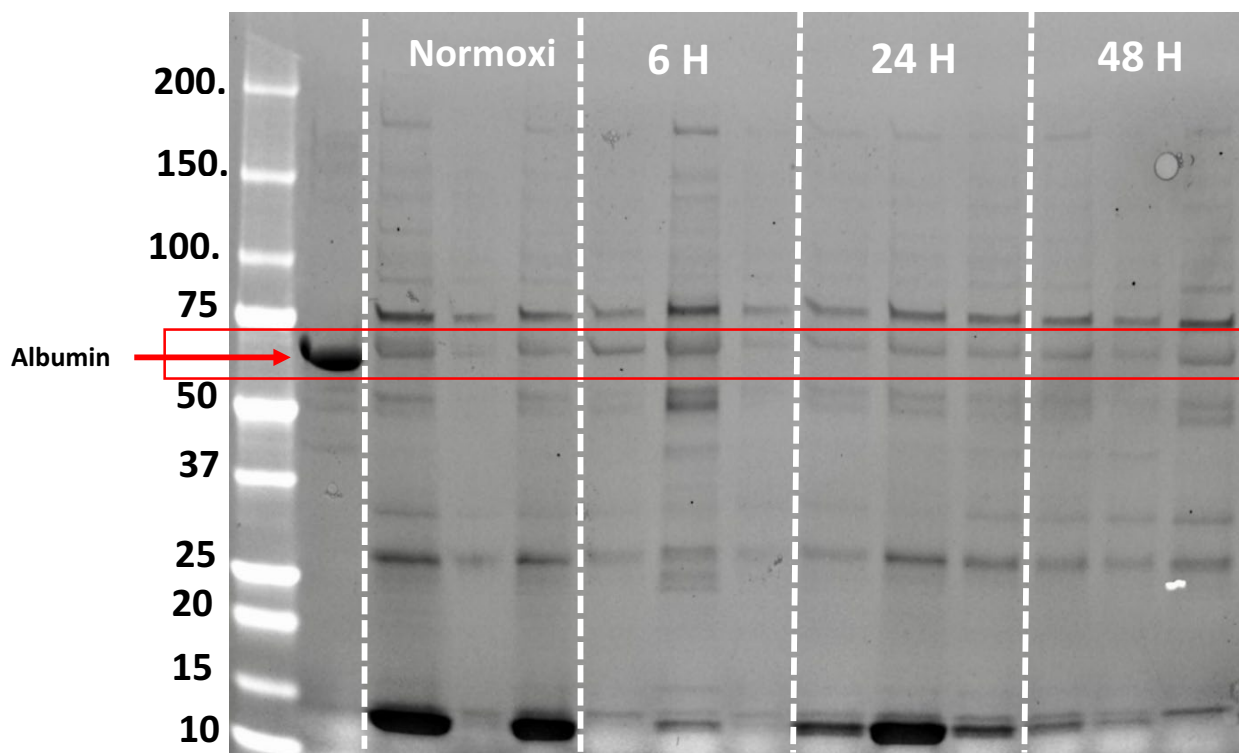
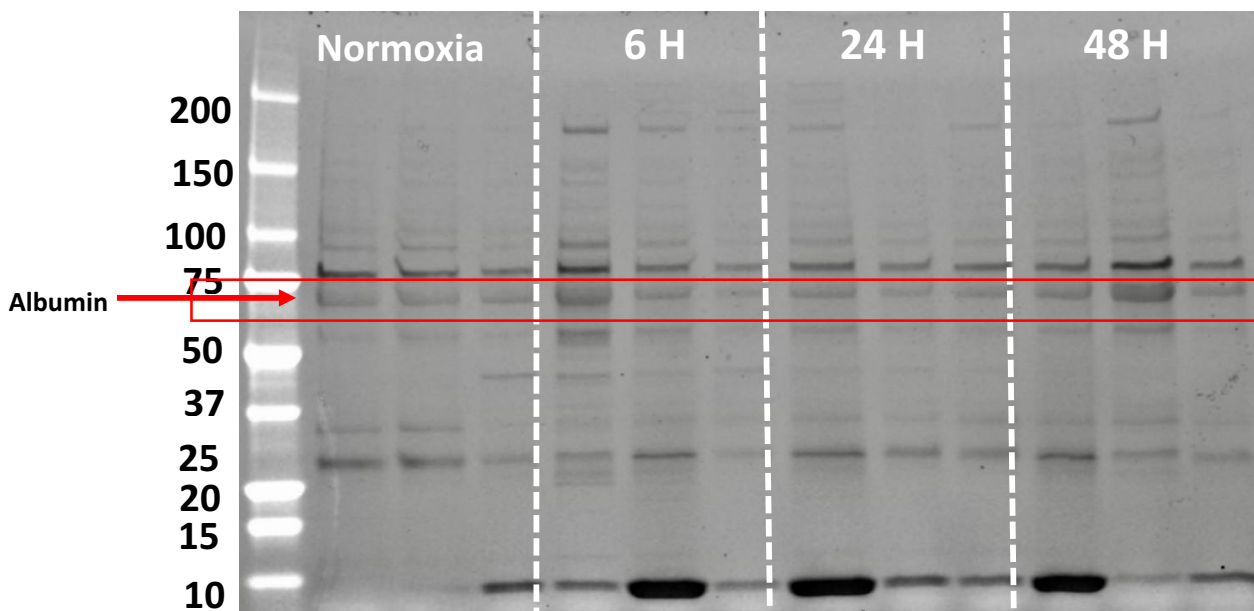


**Fig. 3** Iba1-positive cells in the CPs during hypoxemia with/without peripheral TNF $\alpha$  inhibition, and protein concentration in CSF and plasma during 6, 24, and 48 h hypoxemia. Pannel **A**. images **A–C** are typical images obtained from the sections of the brain taken after normoxia (N), 48 h hypoxemia (H48) and 48 h hypoxemia with TNF $\alpha$  signaling inhibition (H48 + Etanercept), respectively. Macrophages were stained with Iba-1 (green). **B**. The total number of Iba1-positive cells/mm<sup>2</sup> were compared between the three groups; Sign \*\* means  $p < 0.01$ . **C**. Effect of hypoxemia on protein concentration of CSF (square data points) and plasma (circle data points); sign \* means  $p < 0.05$ . **D**. The ratio of CSF albumin/total CSF protein densities. One-way ANOVA analysis followed by Tukey test for multiple comparisons revealed that, duration of hypoxemia exerted significant effect on albumin/total CSF protein ratio ( $p < 0.01$ ). The ratio after 6 h was significantly higher than the ration in normoxia ( $p < 0.05$ ). **E** and **F**. SDA-PAGE electrophoresis of CSF proteins;  $n = 3/\text{group}$  in each figure. The red square highlights the albumin bands in all groups



E



F

Fig. 3 continued

### Effects of hypoxemia on the morphology of CPs

We used TEM to analyze the ultrastructure of CPs collected after normoxia or after 48 h hypoxemia. Typical

images are presented in Fig. 2E; the CP epithelium after normoxia revealed typical features of secretory epithelia, with a lot of microvilli on the apical (CSF) side (solid

black arrows), a lot of mitochondria in the cytoplasm (solid white arrows) and nucleus with a prominent nucleolus (dashed white arrow) and dense chromatin (dashed red arrow). The ultrastructure of the CP epithelium had changed after hypoxemia in all samples (a typical image is presented in Fig. 2F). The microvilli were reduced, appearing as chains of small vacuoles (black solid arrows), while mitochondria became scarce and small (solid white arrows). The nucleoli have disappeared, and the chromatin was no longer visible (dashed red arrow). A lot of vacuoles in the cytoplasm were visible (dashed yellow arrows), which could indicate advanced apoptosis.

### Effects of hypoxemia on the number of the CP macrophages

The density of macrophages in the CPs after normoxia, hypoxemia and hypoxemia with application of Etanercept were  $786.9 \pm 220$  cells/mm<sup>2</sup> (n=6),  $368 \pm 85.7$  cells/mm<sup>2</sup> (n=5) and  $709.4 \pm 109.4$  cells/mm<sup>2</sup> (n=5). Typical images from the three groups are presented in Fig. 3A. There was a significant effect of this protocol on the density of macrophages in the CPs ( $F(2, 12) = 11.01$ ,  $p < 0.01$ ). Pair-wise comparison revealed significant difference between hypoxemia without inhibitor and normoxia ( $p < 0.01$ ) and between hypoxemia with and without inhibitor ( $p < 0.01$ ) (Fig. 3B).

### Effect of hypoxemia on CSF and plasma proteins

In normal conditions, the CSF protein concentration is low, around 0.5–1% of the plasma proteins or  $\approx 0.4$ – $0.8$  g/L. The duration of hypoxemia exerted a significant effect on the protein concentration in the CSF ( $F(3,20) = 7.77$ ,  $n = 6$ /group,  $p < 0.05$ ), but did not exert any significant effect on total protein concentration in plasma ( $F(3,13) = 1.72$ ,  $p > 0.05$ ) (Fig. 3C). Total protein concentration in the CSF significantly increased after 6 h hypoxemia ( $1.96 \pm 0.4$  g/L,  $n = 6$  vs.  $0.98 \pm 0.4$  g/L,  $n = 5$  after normoxia,  $p < 0.01$ ) (Fig. 3C, squares). After 24 and 48 h hypoxemia, the concentrations were  $1.05 \pm 0.21$  g/L ( $n = 6$ ) and  $1.44 \pm 0.69$  g/L ( $n = 6$ ), which was marginally but not significantly higher from the concentrations after normoxia ( $p > 0.05$ , Fig. 3C). Gel electrophoreses of the CSF protein ( $n = 6$ /group) are shown in Fig. 3E, F;  $n$  was 3 in each figure, so the total number of 6 gels/group were done. Hypoxemia duration exerted significant effect on the ratio albumin band density/total CSF protein bands densities ( $F(3,20) = 5.195$ ,  $p < 0.01$ , Fig. 3D). There was a significant increase in the CSF albumin band density/total CSF protein bands densities after 6 h hypoxemia ( $0.096 \pm 0.06$  vs.  $0.017 \pm 0.006$  normoxia,  $p < 0.05$ ), which could indicate a disturbance in the BCSFB and the subsequent albumin leakage into the CSF. In some cases, thick bands of pre-albumins appeared on the blots

( $MW \approx 12$ – $15$  kDa), but these could not be associated to a specific experimental group.

### Effects of hypoxemia on the concentration of cytokines in the CSF and plasma

We could detect 32 cytokines in all CSF samples during normoxia ( $n = 5$ ), 24 h hypoxemia ( $n = 5$ ), 48 h hypoxemia ( $n = 6$ ), and after 1 day recovery ( $n = 6$ ) (Fig. 4A). The highest concentration in the CSF (ng/ml) were of Follistatin-like Protein 1 (FSTL1), which was followed by Serum IFN- $\gamma$ -induced Protein of 10 kDa (IP-10) ( $10^2$  pg/ml) and VEGF ( $10^2$  pg/ml). Fractalkine, Regulated upon Activation Normal T cell Expressed and Presumably Secreted cytokine (RANTES), Irisin, Osteocrin, Secreted Protein Acidic and Rich in cysteine (SPARC) were all present in the range of  $10^1$  pg/ml (Fig. 4A). The concentrations of the remaining 25 cytokines were, at least in one sample, lower than the range of the standard curve(s) concentrations, therefore, the data were presented as MFI and the minimum detectable concentration (pg/ml) for each of these cytokines is presented in respective panels in Fig. 4A.

Surprisingly, the main effect of hypoxemia was a reduction in the inflammation-related cytokines' concentrations. The duration of hypoxemia exerted a statistically significant reduction in the concentrations of 12 cytokines in the CSF, including FSTL1, IP10, SPARC, interleukin (IL)-17A, IL-15, TNF $\alpha$ , IL-6, Granulocyte-macrophage colony-stimulating factor (GM-CSF), Leukaemia inhibitory factor (LIF), fibroblast growth factor (FGF21), Granulocyte colony-stimulating factor (G-CSF), and TGF- $\beta$  superfamily member myostatin (MSTN or GDF8) ( $F$  values and significance shown in Fig. 3A). The biggest changes were a 3.8-fold decrease in FSTL1 after 48 h hypoxemia and 3.7-fold decrease in IP-10 after 24 h hypoxemia (Fig. 4B). Hypoxemia exerted a statistically significant increase in the concentrations of only two cytokines that are related to hypoxia and not to inflammation, VEGF, and EPO (Fig. 4A), the later increased by 2-folds after 48 h hypoxemia (Fig. 4B). In a separate study (data not shown), we revealed a twofold increase in concentrations of TNF $\alpha$  in the brain ISF after 48 h hypoxemia.

We detected 29 cytokines in the plasma samples taken during normoxia ( $n = 11$ ), 2 h ( $n = 6$ ), 6 h ( $n = 4$ ), 24 h ( $n = 5$ ) and 48 h hypoxemia ( $n = 5$ ) (Fig. 5). The duration of hypoxemia exerted significant effects on the concentrations of 15 plasma cytokines: EPO, RANTES, Osteocrin, Fractalkine, IP-10, IL-6, MIP-1 $\alpha$ , IL-1 $\alpha$ , G-CSF, GM-CSF, GDF8, IFN $\gamma$ , IL-10, VEGF, and IL-18. The most obvious change was a  $>20$ -fold and  $>$ tenfold increase in EPO concentration after 24 h and 48 h, respectively ( $p < 0.001$ ) (Fig. 5B) and a 7-fold increase in FGF21 in

plasma after 24 h. Osteocrin decreased >4 times after 48 h ( $p < 0.01$  vs. normoxia). Concentrations of other cytokines have changed for 2–3 folds.

We estimated CSF/plasma ratio for the detected cytokines. The obtained values are presented in Fig. 5C. It could be seen that the ratio was much larger than 1 for 9 cytokines irrespective of hypoxemia, so it could be assumed that these cytokines were primarily brain or CPs borne. These were VEGF, SPARC, FSTL-1, IFN $\gamma$ , IL-13, GM-CSF, TNF $\alpha$ , IL-17A and IL-6 (Fig. 5C). The ratio for 8 cytokines was much less than 1 irrespective of hypoxemia, so it could be hypothesized that they primarily originated from plasma: EPO, BDNF, IL-15, FGF-21, GDF-8, FRAC, OST and RANTES.

#### Effect of inhibition of hypoxia-related cytokines on cell death

We chose three cytokines for this analysis: EPO, because it was revealed that hypoxemia causes a 10–20-fold increase in plasma and a twofold increase in the CSF; VEGF, because there was a significant increase in the CSF during hypoxemia; and TNF $\alpha$  because there was >two-fold increase in the brain ISF during hypoxemia (data not shown). Inhibition of signaling of either of these cytokines exerted profound effects on the cell death in the CPs and EL (Fig. 6). ICV application of sEPOR was detrimental for the CP epithelium, causing significantly more cell death during hypoxemia ( $41.5 \pm 3.72\%$  with sEPOR vs.  $31.5 \pm 4.68\%$  with a vehicle,  $p < 0.01$ ), but it was protective for ELs ( $13.06 \pm 2.0\%$  with sEPOR vs.  $32.5 \pm 8.2\%$  with a vehicle,  $p < 0.01$ ) (Fig. 6B, D). Inhibition of VEGF signaling exerted protective effects on both CPs ( $13.81 \pm 2.1\%$  Axitinib vs.  $31.72 \pm 4.12\%$  vehicle,  $p < 0.01$ ) (Fig. 6B) and ELs ( $13.81 \pm 2.1\%$  Axitinib vs.  $23.3 \pm 8.0$  vehicle,  $p < 0.05$ ) (Fig. 6D). Peripheral inhibition of soluble TNF receptor doubled cell death in CPs ( $62.54 \pm 10.62\%$  Etanercept vs.  $31.8 \pm 4.1\%$  vehicle,  $p < 0.01$ ) and in EL ( $65.36 \pm 9.93\%$  Etanercept vs.  $30.65 \pm 3.9\%$  vehicle,  $p < 0.01$ ) (Fig. 6B, D).

#### Discussion

There were several studies on effects of hypoxia–ischemia on the CPs/CSF system (for a review see [16]). However, this is to the best of our knowledge the first study that assessed effects of hypoxemia. The conditions of the

study were chosen so that they caused changes in the blood gases that mimicked those found in humans during severe T1RF. One of the hallmarks of T1RF is hypoxemia with PaO $_2$  < 60 mmHg [44]. At 8% O $_2$  in the cabinet and normal barometric pressure, PiO $_2$  was  $\approx$ 60 mmHg, while it was >160 at 21% O $_2$ . No available technique can measure PaO $_2$  or hemoglobin saturation in conscious, freely moving rats. However, as the lungs in these rats were not injured, the alveolar gas equation [45, 46] could be applied. It reveals that under these circumstances partial pressure of O $_2$  in the alveoli was equal to or below 53 mmHg [46]. This calculation considers PaCO $_2$  in the rat [47], water vapor pressure in the airways, and the respiratory quotient in the rats of  $\approx$ 0.8 mmHg [48]. Since PaO $_2$  cannot exceed alveolar oxygen, one can safely assume that PaO $_2$  during these conditions was below 60 mmHg, i.e. similar to those found in humans in severe cases of lung injury (e.g., in cytokine storm—induced pneumonia in SARS-CoV-2 infection [49]).

#### Hypoxemia caused cell death in the CPs and ELs in a time dependent manner.

Our data revealed that the duration of hypoxemia led to a significant increase in cell death within CPs and ELs, which could severely affect CSF production and flow of this fluid. The CPs were more resilient to hypoxemia than the ELs during the first 24 h, which could be explained by the abundance of blood supply to the CPs, that could provide glucose and other substrates for glycolysis. However, after 48 h hypoxemia approximately one-third of the cells in both structures were dead and EL suffered a massive further damage during the recovery period, so that the number of dead cells reached 60%. TEM examination of the CP ultrastructure after 48 h hypoxemia revealed changes in the CP epithelium after hypoxemia that were consistent with apoptotic cell death, including short and often disrupted microvilli, a reduced number of mitochondria, disappearance of the dense chromatin and vacuolization of the cytoplasm. However, we could not find any specimen taken after hypoxemia that had grossly physically disturbed epithelial layer. Nonetheless, there was a significant effect of the duration of hypoxemia on the total CSF protein concentration. Bearing in mind cell death occurring in the choroid plexus and ependymal

(See figure on next page.)

**Fig. 4** Concentration of cytokines in the CSF during normoxia, 24 h, 48 h hypoxemia, and after 1 day recovery from 48 h hypoxemia. The full designations of cytokines are provided in Supplementary Table 1. Pannel **A**. The data were analyzed with Mixed-Measures ANOVA test. Each square represents a single data point. The F value, degree of freedom, and p-value are displayed in the upper margin of each panel. If the data is presented as MFI, the minimum detectable concentration (pg/ml) for such cytokines is presented in the panel. Signs \* indicates the significance between the experimental groups vs. normoxia; \* $p < 0.05$ , \*\* $p < 0.01$ , and \*\*\* $p < 0.001$ . **B**. Fold changes in CSF cytokines concentrations at different time points of hypoxemia relative to normoxia. Ratios > 1 indicated an increase, while ratios < 1 indicated a decrease

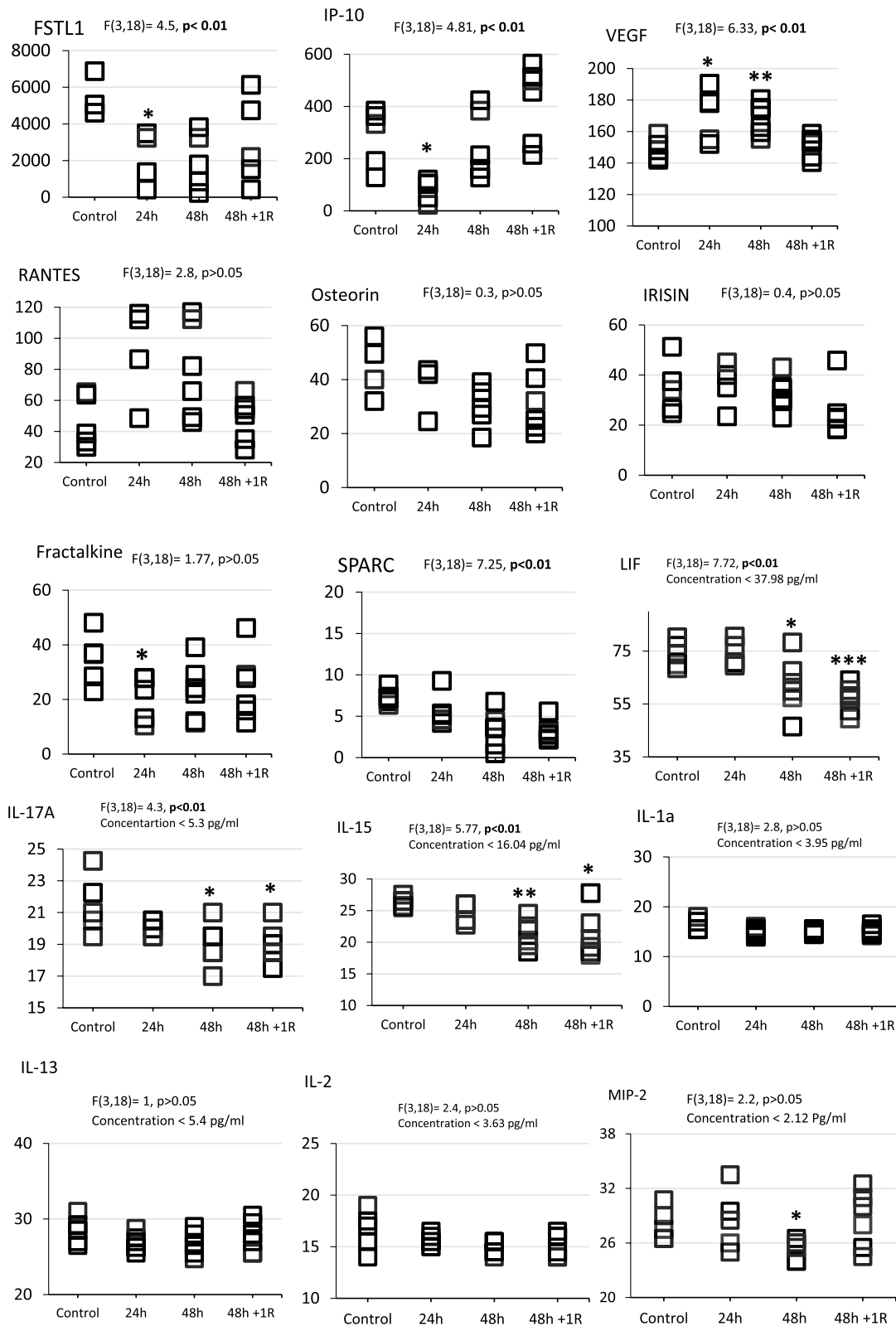


**Fig. 4** (See legend on previous page.)

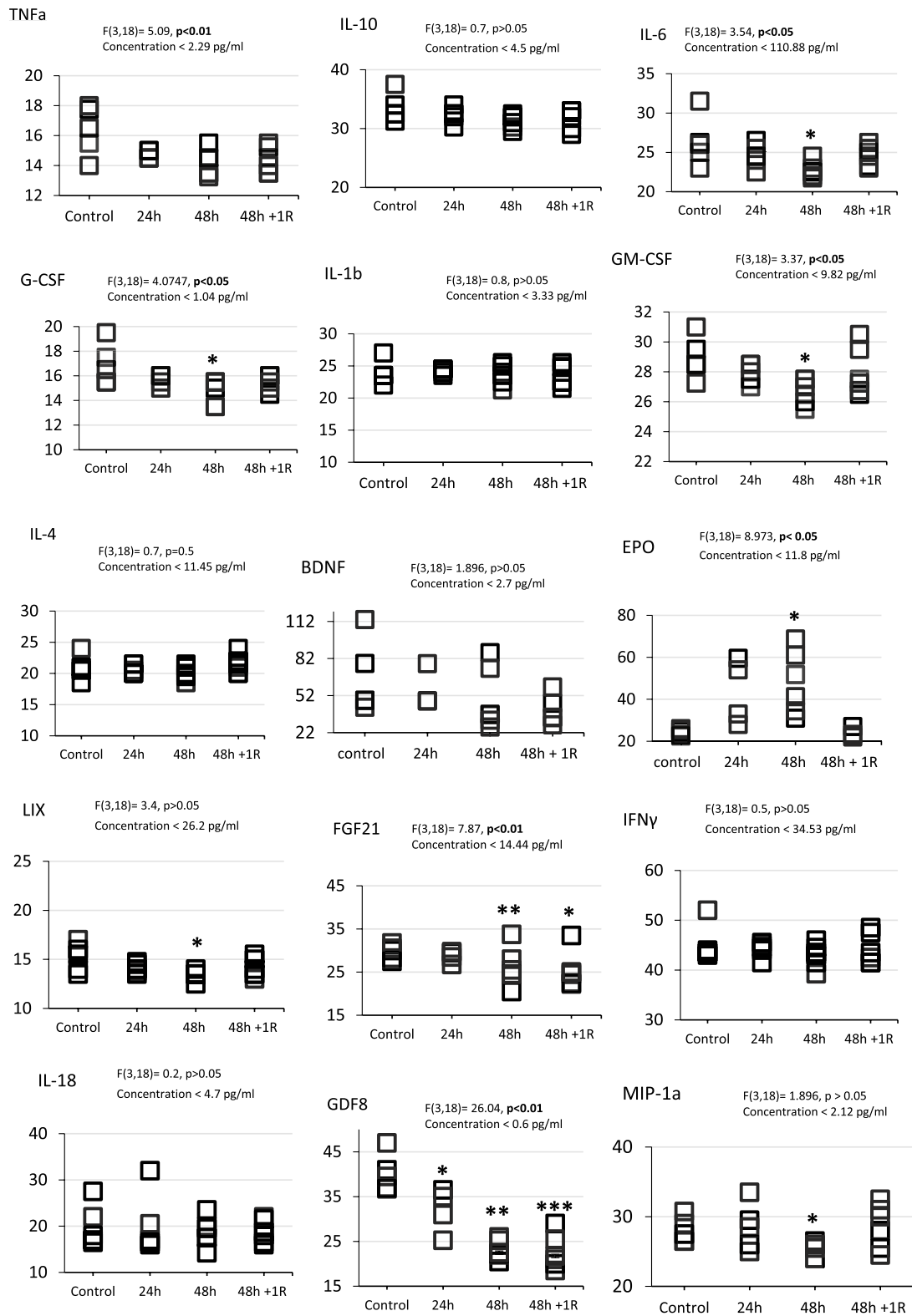
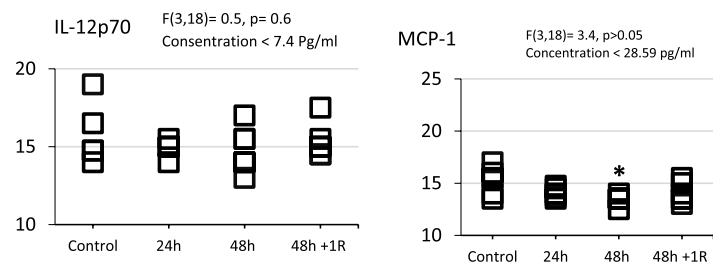
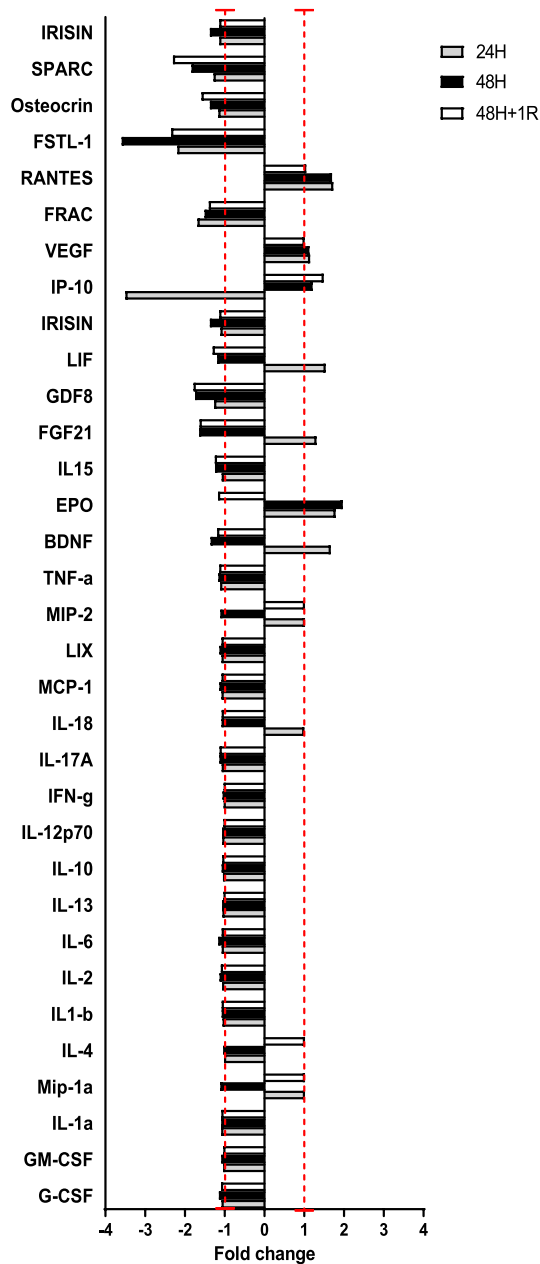


Fig. 4 continued



**A**



**B**

Fig. 4 continued

layer, an increase in the CSF protein levels could be either due to a disruption of the BCSFB (in which case plasma proteins leak into the CSF) or due to a leak of proteins from dead cell. Gel electrophoreses of the CSF protein (Fig. 3E, F) revealed that hypoxemia duration exerted significant effect on the ratio albumin band density/total CSF protein bands density and a significant increase in the CSF albumin band density/total CSF protein bands densities after 6 h hypoxemia. Since albumin is a plasma protein, these data indicate that the primary cause of the CSF protein increase was the BCSFB damage.

However, the mechanism that initiated cell death was less clear. CPs are selectively vulnerable to ischemia [21]. Vulnerability of cells to hypoxia depends on their metabolic demands and dependency on oxidative metabolism. We have revealed that  $PtO_2$  in the premotor cortex, which was  $\approx 50$  mmHg during normoxia, decreased to 6.4 mmHg 1 h after reduction of inspired  $O_2$  to 8% [8], which was well above a threshold of 1 mmHg at which oxidative phosphorylation stops, bearing the affinity of  $O_2$  for Complex 4 [9].

Another cause of cell death in the CPs could be damage of the cells by reactive oxygen species and free radicals. Hypoxia causes HIF—mediated increase in NADPH oxidase activity, thus utilizing NADPH [50] and also it causes electrons premature leak from complex 1 (NADH dehydrogenase) and complex 3 (ubiquinol-cytochrome c reductase), which leads to incomplete reduction of oxygen and formation of superoxide radicals ( $O_2^-$ ) [51, 52]. These radicals are highly reactive and can cause lipid peroxidation and protein oxidation that damages the structural integrity of cell membranes and cause modifications and structural changes of proteins.

#### Hypoxemia and pro-inflammatory cytokines in the CSF.

All CSF samples contained 32 hypoxia- and inflammation-related cytokines, while 29 were present in plasma. However, a pattern of changes in the concentrations in the CSF suggests that hypoxemia largely inhibited rather than initiated inflammatory response in the brain. Nine cytokines that were detected in the CSF were probably brain-borne: VEGF, SPARC, FSTL-1, IFN $\gamma$ , IL-13, GM-CSF, TNF $\alpha$ , IL-17A and IL-6. Duration of hypoxemia

exerted statistically significant decrease in concentrations of 6 of these cytokines: macrophages-secreted GM-CSF, SPARC, which is involved in migration and differentiation [53]), FSTL1, which stimulates release of proinflammatory cytokines [54]) and pro-inflammatory IL-6 and IL-17. Concentrations of proinflammatory cytokines IFN $\gamma$  and IL-13 did not change significantly in the CSF during hypoxemia. The only brain-borne cytokine that increased in the CSF during hypoxemia was VEGF, a chief regulator of neovascularization that is not related to inflammation.

Previous study on mice that also used isobaric hypoxemia (10%  $O_2$ ) for 7 days has revealed that 1 h after 7-days hypoxemia 10 cytokines significantly increased in plasma and 4 increased in the retina homogenates. Based on this data they concluded that the immediate post-hypoxic period was characterized by molecular changes consistent with inflammation [55]. However, a closer look at the data presented in this publication reveals a complex, rather than a clear proinflammatory response, which was likely associated to a long duration of hypoxemia that triggered homeostatic processes aimed to adapt the body to a new, lower,  $PaO_2$ .

Hypoxemia caused a large and significant reduction in the densities of Iba-positive cells in the CPs, which are likely to be either stromal or epiplexus macrophages or monocytes [56]. A decrease in the number of macrophages could indicate their migration across the CP epithelium into the CSF (stromal macrophages), detachment from the CP apical membrane (epiplexus macrophages) or movement across the CP epithelium and endothelium in the blood. This could be triggered by cell death in the CPs or in the ELs. However, this was cancelled out by peripheral inhibition of TNF $\alpha$  signaling, which indicated that the movements of macrophages in the CPs were triggered either by plasma-borne or by the CPs-produced TNF $\alpha$ , possibly via TNF receptor (TNFR)-1 [57].

#### Inhibition of EPO-, VEGF- or TNF $\alpha$ - mediated signaling exerted profound effects on cell death during hypoxemia

We identified three cytokines that increased in the brain extracellular fluids during hypoxemia: EPO, which is

(See figure on next page.)

**Fig. 5** Concentration of cytokines in the plasma during 2, 6, 24, and 48 h hypoxemia. The full designations of cytokines are provided in Supplementary Table 1. Pannel **A**. In one set of rats, samples were collected during normoxia, and after 2 h, and 6 h hypoxemia (squares). In another set, samples were collected during normoxia, and after 24 h and 48 h hypoxemia (triangles). Statistical analysis was carried out using a Mixed Measures ANOVA test; signs indicate: \* - $p < 0.05$ , \*\*— $p < 0.01$ , \*\*\*— $p < 0.001$ . Degrees of freedom and F values were presented in the top of each panel. The upper raw shows statistical analysis for set 1, the lower raw shows statistical analysis for set 2. If the data is presented as MFI, the minimum detectable concentration (pg/ml) for such cytokines is presented in the panel. **B**. Fold changes in the concentrations of cytokines in the plasma at different time points of hypoxemia relative to normoxia; ratio  $> 1$  = increase,  $< 1$  = decrease. **C**. The CSF/Plasma ratio for the detected cytokines during normoxia, and after 24 h and 48 h hypoxemia. *OST* Osteocrin, *FRAC* Fractalkine

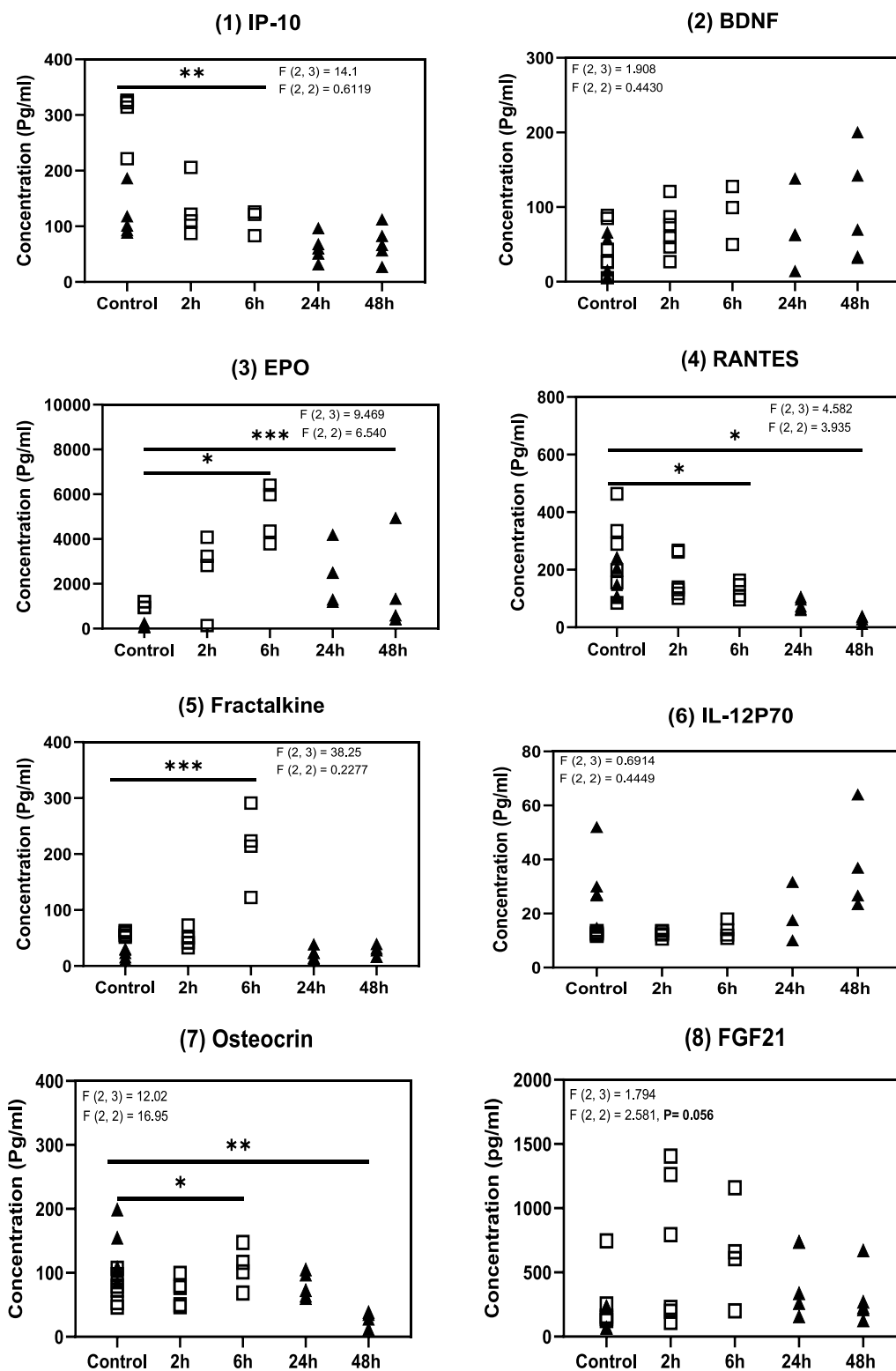


**Fig. 5** (See legend on previous page.)

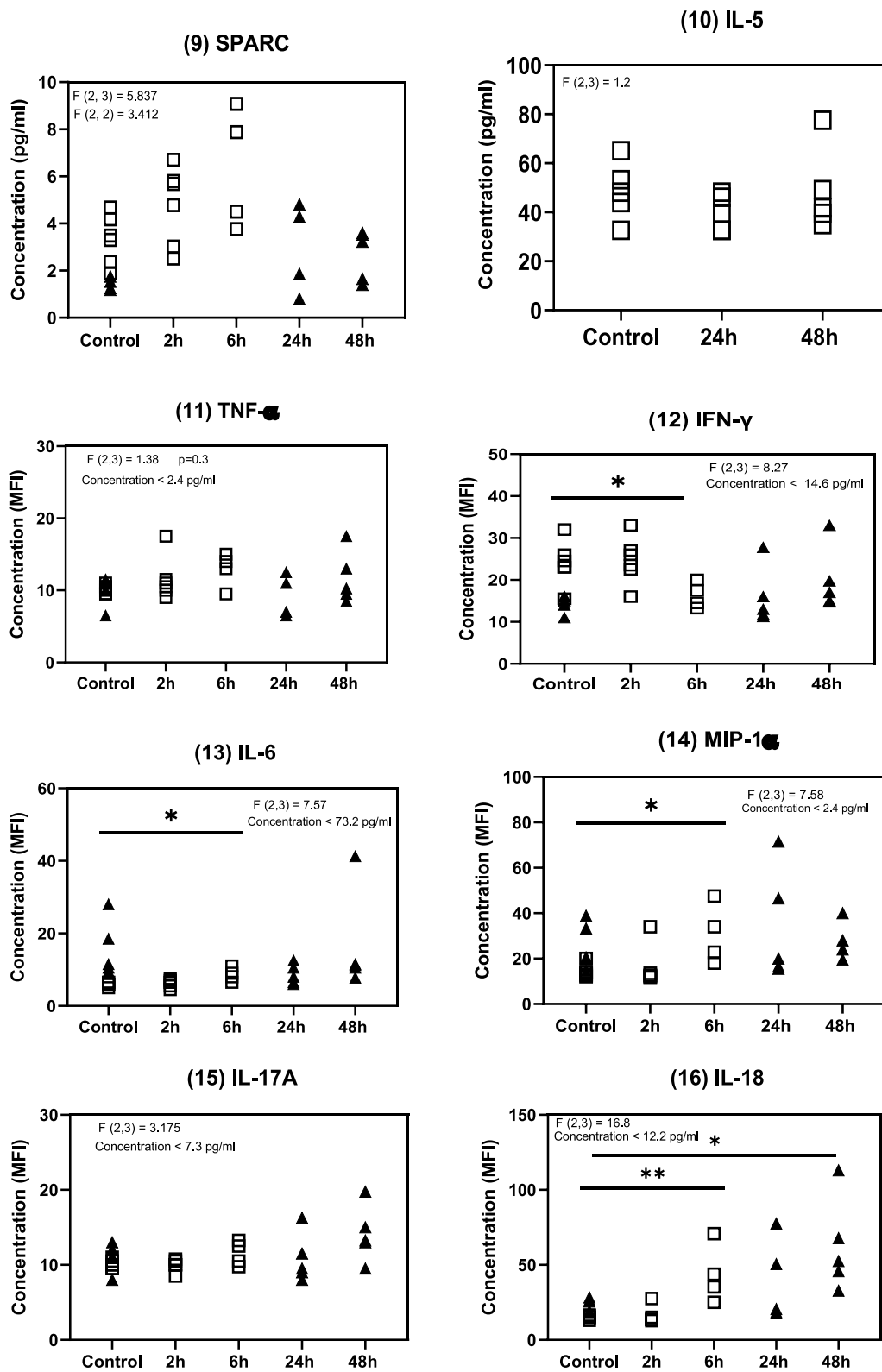


Fig. 5 continued

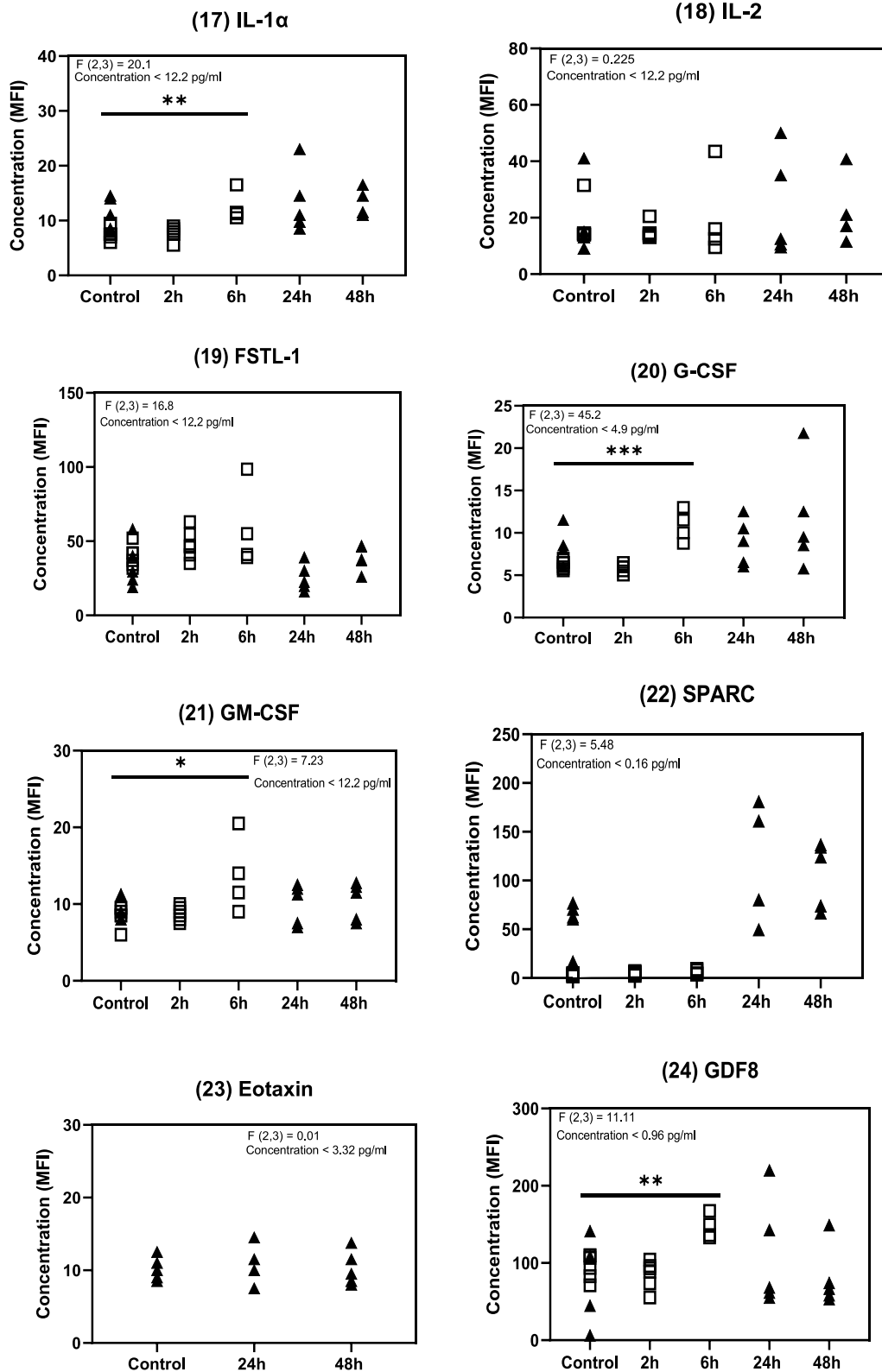
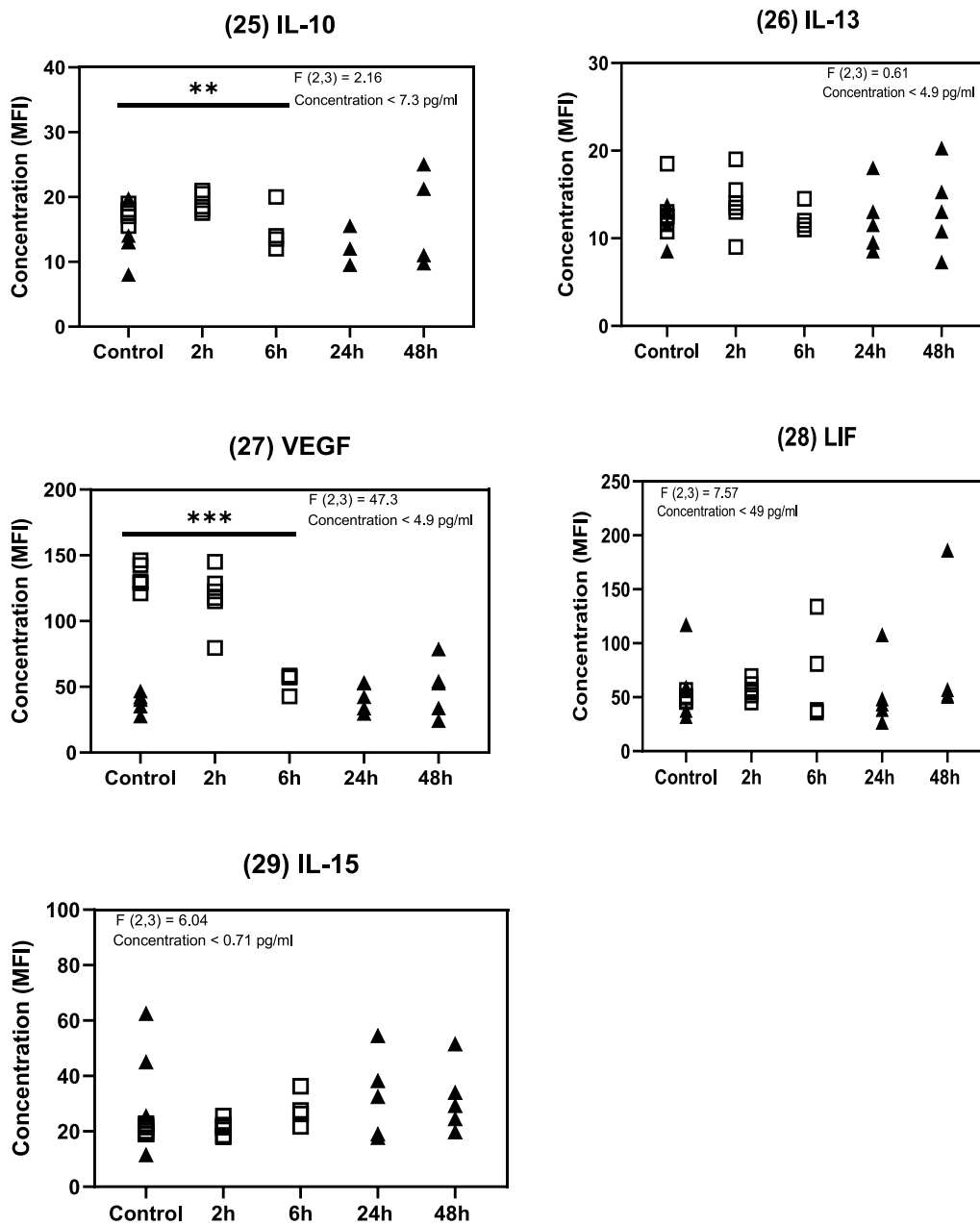


Fig. 5 continued



A

Fig. 5 continued

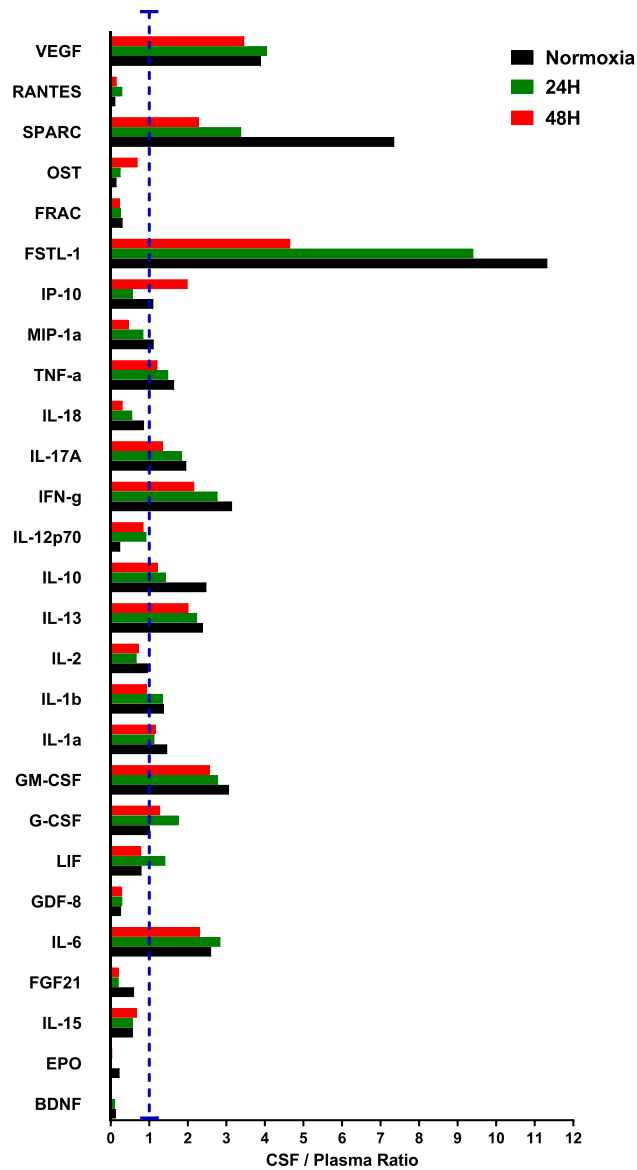
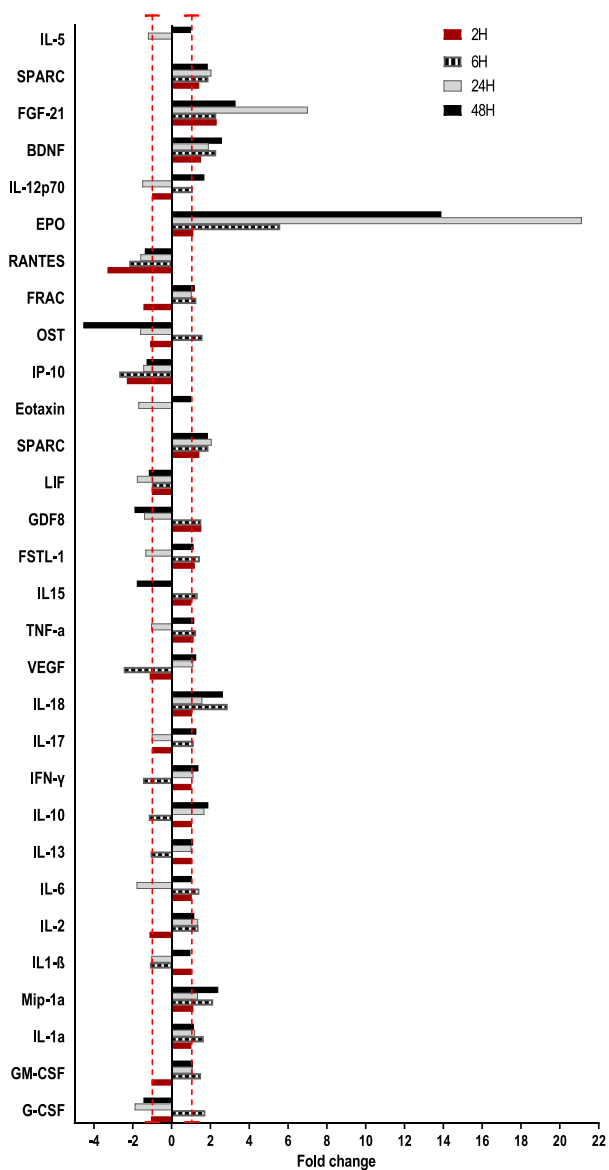
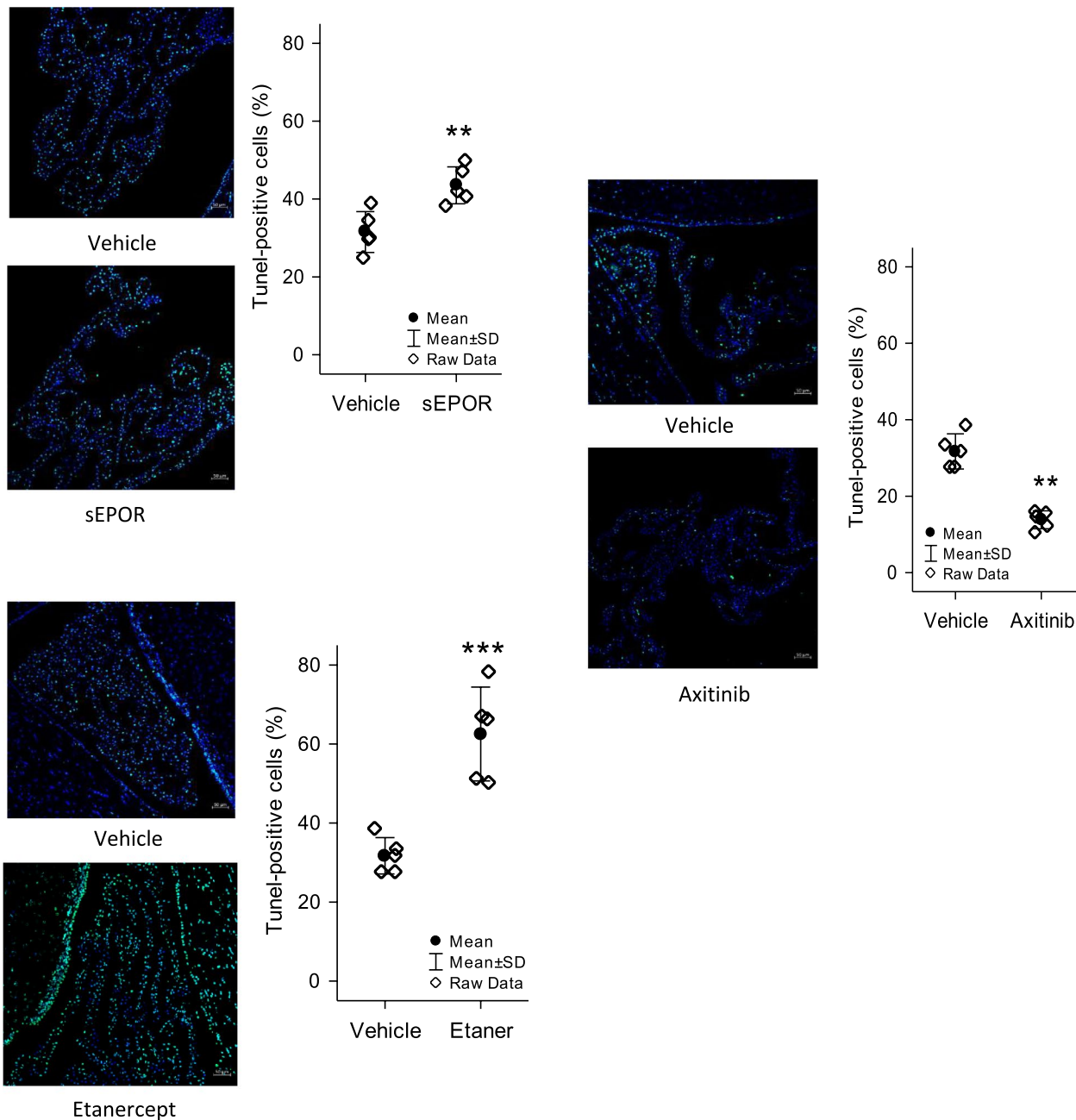


Fig. 5 continued

## LV Choroid Plexuses



**A**

**Fig. 6** Cell death in the CPs and EL after applications of inhibitors. Panels **A** and **B**, typical images of the CP (6A) and EL (6B) following TUNEL staining after hypoxemia, with and without inhibition protocols prior to hypoxemia. Inhibitors were sEPOR (EPO signaling inhibition), Axitinib (VEGF signaling inhibition), and Etanercept (Etanercept; TNF $\alpha$  signaling inhibition). Nuclei are stained with DAPI (blue), while TUNEL-positive cells (indicating cell death) are shown in green. Scale bar: 50  $\mu$ m. Arrows in 6B highlight the EL. Graphs in **A** and **B** the graphs to the right of each inhibition protocol display raw data for each group alongside the mean  $\pm$  SD. Asterisks (\*) indicate significant differences between the experimental group and its corresponding vehicle: \* $p < 0.05$ , \*\* $p < 0.01$ , \*\*\* $p < 0.001$

### Ependymal Layer

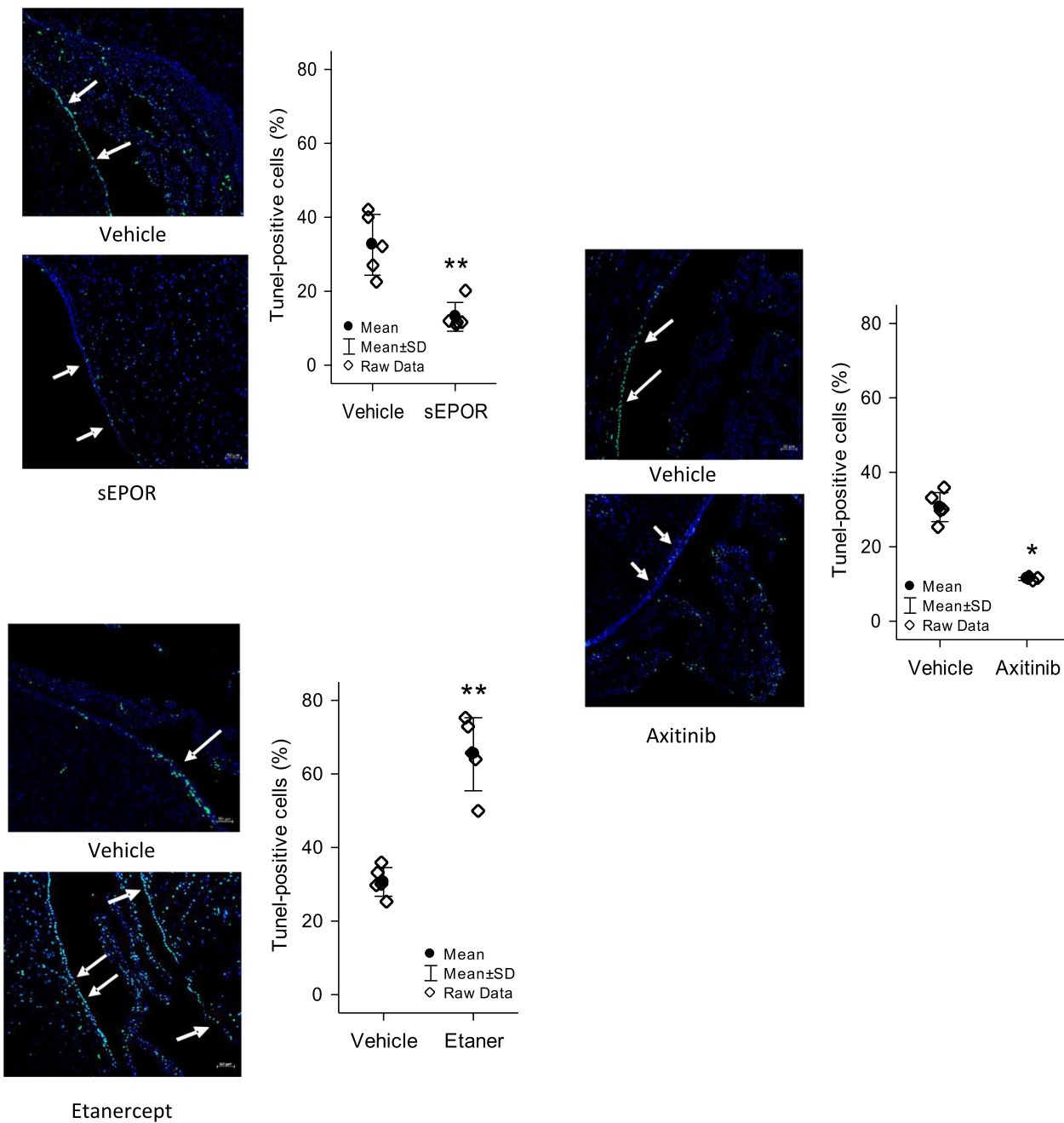


Fig. 6 continued

a major anti-apoptotic cytokine [58, 59], VEGF, that is a key regulator of neovascularization [60] and TNF $\alpha$ , which is a major pro-inflammatory cytokine [61].

### B

The soluble receptor binds EPO with ED<sub>50</sub> 60–300 ng/mL [62]. ICV injection of sEPOR increased the number of dead cells in the CPs, but, surprisingly, it caused a significant reduction in the number of dead cells in EL

after 48 h hypoxemia. Though EPO signaling is generally considered as protective and anti-apoptotic in cerebral ischemia [63], EPO could also exert injurious effects [64]. Mortality in stroke patients that received EPO increased compared to placebo [65], thus, it was concluded that application of rEPO to these patients is not recommended [66, 67]. Another explanation for our findings could be that EPOR-associated JAK-2-induced phosphorylation and activation of the signal transducer and activator of transcription 5 (STAT-5) [68, 69], mediated the upregulation of pyruvate dehydrogenase kinase [70, 71], which could shift more glycolysis-derived pyruvate into the Krebs cycle, thereby increasing free radical production [72] that may damage cells [51, 52].

Axitinib is a highly selective inhibitor of VEGFR tyrosine kinase 1, 2, and 3. Cell death in the CPs and EL was reduced after 24 h when applying Axitinib, which suggested that VEGF signaling is detrimental to these cells during hypoxemia. This effect could be partially explained by the fact that VEGF is a mitogen associated with angiogenesis, which enhances mitochondrial oxidative respiration [73]. In the settings of limited oxygen supply, that could cause oxidative stress and be detrimental for the cells. Additionally, a study on metabolic effects of VEGF revealed that this cytokine could uncouple mitochondrial oxidation from ATP production [74], so that O<sub>2</sub> consumption could increase disproportionately to ATP production, which could also be detrimental when oxygen availability is limited.

Application of Etanercept increased the number of TUNEL-positive cells increased in both CPs and EL. This suggested that TNF $\alpha$ -mediated signaling was protective to these cells during hypoxemia. TNF $\alpha$  signaling via TNFR1 exerts proinflammatory and pro-apoptotic effects, whereas signaling via TNFR2 promotes protective effects [75]. Activation of TNFR2 anti-inflammatory pathways was revealed in microglia in hypoxic conditions [76]. As Etanercept lowers the available TNE, we hypothesize that the observed effects of peripheral application of Etanercept would lower TNF $\alpha$  in plasma to marginal amounts, so that this cytokine predominantly exerted its action through higher affinity, pro-apoptotic TNFR1, rather than through lower affinity, anti-apoptotic TNFR2.

In summary, this study revealed that 48 h hypoxemia exerts detrimental effects on the CPs and CSF system, which could have profound effects on the CSF production and brain ECFs composition and flow. Cell death was modulated by the hypoxia- and inflammation-related cytokines. However, pattern of changes in the concentrations of the CSF cytokines did not suggest that 48 h hypoxemia triggered inflammatory response in the brain.

## Abbreviations

BCSFB	Blood-cerebrospinal fluid barrier
CSF	Cerebrospinal fluid
DAPI	4',6-Diamidino-2-phenylindole
ECFs	Extracellular fluids
EL	Ependymal lining
EPO	Erythropoietin
FSTL1	Follistatin-like protein 1
GM-CSF	Granulocyte-macrophage colony-stimulating factor
ICV	Intracerebroventricular
IFN $\gamma$	Interferon Gamma
IL	Interleukin
ISF	Interstitial fluid
NO	Nitric oxide
PaO <sub>2</sub>	Partial pressure of arterial oxygen
PiO <sub>2</sub>	Partial pressure of inspired oxygen
PtO <sub>2</sub>	Partial pressure of tissue oxygen
sABI	Secondary acquired brain injury
SPARC	Secreted protein acidic and rich in cysteine
TEM	Transmission electron microscopy
TUNEL	Terminal Deoxynucleotidyl Transferase dUTP Nick-End Labeling
TNF $\alpha$	Tumor necrosis factor alpha
VEGF	Vascular endothelial growth factor
HIF	Hypoxia-inducible factor

## Supplementary Information

The online version contains supplementary material available at <https://doi.org/10.1186/s12987-024-00613-w>.

Additional file 1.

## Acknowledgements

We acknowledge help of Dr. Marian Turcani in the statistical analysis, Dr. Ghanim Al-Khaledi in jugular vein catheterization, Ms. Susan Varges for the TUNEL assay, Ms. Mini Varghese and Ms. Sajida Tappa for CSF protein estimation and electrophoresis and Ms. Jessy Mathew for acquiring TEM images.

## Author contributions

Zoran Redzic contributed to the study conception and design. Material preparation, data collection and analysis were performed by Rawan Barakat, Hameed Al-Sarraf and Zoran Redzic. The first draft of the manuscript was written by Zoran Redzic and all authors commented on previous versions of the manuscript. All authors read and approved the final manuscript.

## Funding

This work was supported by the Kuwait University Research Sector Grant no MY 02-18 and GM 01-15.

## Availability of data and materials

The datasets generated during and/or analyzed during the current study are available in the Figshare repository, [<https://doi.org/10.6084/m9.figshare.26056114>].

## Declarations

### Ethics approval and consent to participate

The Institutional Animal Ethics Committee approved all experimental protocols, which comply with the National Research Council's Guide for the care and use of laboratory animals. The letter of ethical approval was issued on 01. June 2019.

### Consent for publication

Not applicable.

### Competing interests

The authors declare no competing interests.

Received: 12 September 2024 Accepted: 20 December 2024  
Published online: 12 March 2025

## References

- Henig NR, Pierson DJ. Mechanisms of hypoxemia. *Respir Care Clin N Am*. 2000;6(4):501–21.
- Huang X, Hussain B, Chang J. Peripheral inflammation and blood-brain barrier disruption: effects and mechanisms. *CNS Neurosci Ther*. 2021;27(1):36–47.
- Ziaka M, Exadaktylos A. ARDS associated acute brain injury: from the lung to the brain. *Eur J Med Res*. 2022;27(1):150.
- Tzotzos SJ, Fischer B, Fischer H, Zeitlinger M. Incidence of ARDS and outcomes in hospitalized patients with COVID-19: a global literature survey. *Crit Care*. 2020;24(1):516.
- Brownlee W, Bourdette D, Broadley S, Killestein J, Ciccarelli O. Treating multiple sclerosis and neuromyelitis optica spectrum disorder during the COVID-19 pandemic. *Neurology*. 2020;94(22):949–52.
- Huang M, Gedansky A, Hassett CE, Price C, Fan TH, Stephens RS, et al. Pathophysiology of brain injury and neurological outcome in acute respiratory distress syndrome: a scoping review of preclinical to clinical studies. *Neurocrit Care*. 2021;35(2):518–27.
- Solomon IH, Normandin E, Bhattacharyya S, Mukerji SS, Keller K, Ali AS, et al. Neuropathological features of Covid-19. *N Engl J Med*. 2020;383(10):989–92.
- Barakat RM, Turcani M, Al-Khaledi G, Kilarkaje N, Al-Sarraf H, Sayed Z, et al. Low oxygen in inspired air causes severe cerebrocortical hypoxia and cell death in the cerebral cortex of awake rats. *Neurosci Lett*. 2024;818:137515.
- Kadenbach B, Complex IV. The regulatory center of mitochondrial oxidative phosphorylation. *Mitochondrion*. 2021;58:296–302.
- Redzic Z. Molecular biology of the blood-brain and the blood-cerebrospinal fluid barriers: similarities and differences. *Fluids Barriers CNS*. 2011;8(1):3.
- Hladky SB, Barrand MA. Mechanisms of fluid movement into, through and out of the brain: evaluation of the evidence. *Fluids Barriers CNS*. 2014;11(1):26.
- Damkier HH, Brown PD, Praetorius J. Cerebrospinal fluid secretion by the choroid plexus. *Physiol Rev*. 2013;93(4):1847–92.
- Rasmussen MK, Mestre H, Nedergaard M. Fluid transport in the brain. *Physiol Rev*. 2022;102(2):1025–151.
- Chodobski A, Szmydynger-Chodobska J. Choroid plexus: target for polypeptides and site of their synthesis. *Microsc Res Tech*. 2001;52(1):65–82.
- Lepko T, Pusch M, Müller T, Schulte D, Ehse J, Kiebler M, et al. Choroid plexus-derived miR-204 regulates the number of quiescent neural stem cells in the adult brain. *Embo J*. 2019;38(17):e100481.
- Xiang J, Routh LJ, Wilkinson DA, Hua Y, Moos T, Xi G, et al. The choroid plexus as a site of damage in hemorrhagic and ischemic stroke and its role in responding to injury. *Fluids Barriers CNS*. 2017;14(1):8.
- Maślińska D, Laure-Kamionowska M, Taraszewska A, Deręgowski K, Maśliński S. Immunodistribution of amyloid beta protein (A $\beta$ ) and advanced glycation end-product receptors (RAGE) in choroid plexus and ependyma of resuscitated patients. *Folia Neuropathol*. 2011;49(4):295–300.
- Pulsinelli WA, Brierley JB, Plum F. Temporal profile of neuronal damage in a model of transient forebrain ischemia. *Ann Neurol*. 1982;11(5):491–8.
- Kaur C, Sivakumar V, Ling EA. Melatonin protects periventricular white matter from damage due to hypoxia. *J Pineal Res*. 2010;48(3):185–93.
- Rothstein RP, Levison SW. Damage to the choroid plexus, ependyma and subependyma as a consequence of perinatal hypoxia/ischemia. *Dev Neurosci*. 2002;24(5):426–36.
- Ennis SR, Keep RF. The effects of cerebral ischemia on the rat choroid plexus. *J Cereb Blood Flow Metab*. 2006;26(5):675–83.
- Marín-Teva JL, Cuadros MA, Martín-Oliva D, Navascués J. Microglia and neuronal cell death. *Neuron Glia Biol*. 2011;7(1):25–40.
- Luo Z, Tian M, Yang G, Tan Q, Chen Y, Li G, et al. Hypoxia signaling in human health and diseases: implications and prospects for therapeutics. *Signal Transduct Target Ther*. 2022;7(1):218.
- Mitroshina EV, Savyuk MO, Ponimaskin E, Vedunova MV. Hypoxia-inducible factor (HIF) in ischemic stroke and neurodegenerative disease. *Front Cell Dev Biol*. 2021;9:703084.
- Dunn JF, Isaacs AM. The impact of hypoxia on blood-brain, blood-CSF, and CSF-brain barriers. *J Appl Physiol*. 2021;131(3):977–85.
- Ghasemi A, Jeddi S, Kashfi K. The laboratory rat: age and body weight matter. *Excli j*. 2021;20:1431–45.
- Lombardi C, Meriggi P, Agostoni P, Faini A, Bilo G, Revera M, et al. High-altitude hypoxia and periodic breathing during sleep: gender-related differences. *J Sleep Res*. 2013;22(3):322–30.
- Mortola JP. Gender and the circadian pattern of body temperature in normoxia and hypoxia. *Respir Physiol Neurobiol*. 2017;245:4–12.
- Nijboer CH, Groenendaal F, Kavelaars A, Hagberg HH, van Bel F, Heijnen CJ. Gender-specific neuroprotection by 2-iminobiotin after hypoxia-ischemia in the neonatal rat via a nitric oxide independent pathway. *J Cereb Blood Flow Metab*. 2007;27(2):282–92.
- Hill CA, Fitch RH. Sex differences in mechanisms and outcome of neonatal hypoxia-ischemia in rodent models: implications for sex-specific neuroprotection in clinical neonatal practice. *Neurol Res Int*. 2012;2012:867531.
- Feng J, Fitz Y, Li Y, Fernandez M, Cortes Puch I, Wang D, et al. Catheterization of the carotid artery and jugular vein to perform hemodynamic measures, infusions and blood sampling in a conscious rat model. *J Vis Exp*. 2015. <https://doi.org/10.3791/51881-v>.
- Al-Sarraf H, Preston JE, Segal MB. Acidic amino acid clearance from CSF in the neonatal versus adult rat using ventriculo-cisternal perfusion. *J Neurochem*. 2000;74(2):770–6.
- Barthel L, Engler H, Hadamitzky M, Lückemann L, Sure U, Schedlowski M, et al. A step-by-step guide for microsurgical collection of uncontaminated cerebrospinal fluid from rat cisterna magna. *J Neurosci Methods*. 2021;352:109085.
- Dalman MR, Deeter A, Nimishakavi G, Duan ZH. Fold change and p-value cutoffs significantly alter microarray interpretations. *BMC Bioinform*. 2012;13(Suppl 2):S11.
- Yang IV, Chen E, Hasseman JP, Liang W, Frank BC, Wang S, et al. Within the fold: assessing differential expression measures and reproducibility in microarray assays. *Genome Biol*. 2002;3(11):research0062.
- Aguilan JT, Kulej K, Sidoli S. Guide for protein fold change and p-value calculation for non-experts in proteomics. *Mol Omics*. 2020;16(6):573–82.
- Pagnuzzi-Boncompagni M, Picco V, Vial V, Planas-Bielsa V, Vandenberghe A, Daubon T, et al. Antiangiogenic compound axitinib demonstrates low toxicity and antitumoral effects against medulloblastoma. *Cancers*. 2021. <https://doi.org/10.3390/cancers14010070>.
- Smith BJ, Pithavala Y, Bu HZ, Kang P, Hee B, Deese AJ, et al. Pharmacokinetics, metabolism, and excretion of [14C]axitinib, a vascular endothelial growth factor receptor tyrosine kinase inhibitor, in humans. *Drug Metab Dispos*. 2014;42(5):918–31.
- Tracey D, Klareskog L, Sasso EH, Salfeld JG, Tak P. Tumor necrosis factor antagonist mechanisms of action: a comprehensive review. *Pharmacol Ther*. 2008;117(2):244–79.
- Sheen JM, Chen YC, Hsu MH, Tain YL, Yu HR, Huang LT. Combined intraperitoneal and intrathecal etanercept reduce increased brain tumor necrosis factor-alpha and asymmetric dimethylarginine levels and rescues spatial deficits in young rats after bile duct ligation. *Front Cell Neurosci*. 2016;10:167.
- Yildirim Y, Cellad EG, Kara AV, Yilmaz Z, Kadiroglu AK, Bahadır MV, et al. Effect of intraperitoneal etanercept on oxidative stress in rats with peritonitis. *Oxid Med Cell Longev*. 2016;2016:9418468.
- Lee BY, Kwon KI, Kim MS, Baek IH. Michaelis-menten elimination kinetics of etanercept, rheumatoid arthritis biologics, after intravenous and subcutaneous administration in rats. *Eur J Drug Metab Pharmacokinet*. 2016;41(4):433–9.
- Vidal L, Pinsach J, Striedner G, Caminal G, Ferrer P. Development of an antibiotic-free plasmid selection system based on glycine auxotrophy for recombinant protein overproduction in *Escherichia coli*. *J Biotechnol*. 2008;134(1–2):127–36.
- Mirabile VS, Shebl E, Sankari A, Burns B. Respiratory failure in adults. Treasure Island: StatPearls Publishing; 2024.
- Sharma S, Hashmi MF, Burns B. Alveolar gas equation. Treasure Island: StatPearls Publishing; 2024.

46. Bartlett JG, Faling LJ, Willey S. Quantitative tracheal bacteriologic and cytologic studies in patients with long-term tracheostomies. *Chest*. 1978;74(6):635–9.
47. Liu X, Li C, Falck JR, Harder DR, Koehler RC. Relative contribution of cyclooxygenases, epoxyeicosatrienoic acids, and pH to the cerebral blood flow response to vibrissal stimulation. *Am J Physiol Heart Circ Physiol*. 2012;302(5):H1075–85.
48. Berg KM, Donnino MW, Callaway C. Looking for CO(2): exploring the novel finding of low respiratory quotient after cardiac arrest. *J Am Heart Assoc*. 2018. <https://doi.org/10.1161/JAHA.118.009500>.
49. Visca D, Migliori GB, Dinh-Xuan AT, Centis R, Belli S, Vitacca M, et al. The role of blood gas analysis in the post-acute phase of COVID-19 pneumonia. *Arch Bronconeumol*. 2022;58(6):513–6.
50. Chen R, Lai UH, Zhu L, Singh A, Ahmed M, Forsyth NR. Reactive oxygen species formation in the brain at different oxygen levels: the role of hypoxia inducible factors. *Front Cell Dev Biol*. 2018;6:132.
51. Nickel A, Kohlhaas M, Maack C. Mitochondrial reactive oxygen species production and elimination. *J Mol Cell Cardiol*. 2014;73:26–33.
52. Tirichen H, Yaigoub H, Xu W, Wu C, Li R, Li Y. Mitochondrial reactive oxygen species and their contribution in chronic kidney disease progression through oxidative stress. *Front Physiol*. 2021;12:627837.
53. Bradshaw AD, Sage EH. SPARC, a matricellular protein that functions in cellular differentiation and tissue response to injury. *J Clin Invest*. 2001;107(9):1049–54.
54. Chaly Y, Hostager B, Smith S, Hirsch R. Follistatin-like protein 1 and its role in inflammation and inflammatory diseases. *Immunol Res*. 2014;59(1–3):266–72.
55. Mesentier-Louro LA, Rangel B, Stell L, Shariati MA, Dalal R, Nathan A, et al. Hypoxia-induced inflammation: profiling the first 24-hour posthypoxic plasma and central nervous system changes. *PLoS ONE*. 2021;16(3):e0246681.
56. Cui J, Xu H, Lehtinen MK. Macrophages on the margin: choroid plexus immune responses. *Trends Neurosci*. 2021;44(11):864–75.
57. D'Mello C, Le T, Swain MG. Cerebral microglia recruit monocytes into the brain in response to tumor necrosis factor- $\alpha$  signaling during peripheral organ inflammation. *J Neurosci*. 2009;29(7):2089–102.
58. Nairz M, Sonnweber T, Schroll A, Theurl I, Weiss G. The pleiotropic effects of erythropoietin in infection and inflammation. *Microbes Infect*. 2012;14(3):238–46.
59. Suresh S, Rajvanshi PK, Noguchi CT. The many facets of erythropoietin physiologic and metabolic response. *Front Physiol*. 2019;10:1534.
60. Nieves BJ, D'Amore PA, Bryan BA. The function of vascular endothelial growth factor. *BioFactors*. 2009;35(4):332–7.
61. van Loo G, Bertrand MJM. Death by TNF: a road to inflammation. *Nat Rev Immunol*. 2023;23(5):289–303.
62. Kitamura T, Tange T, Terasawa T, Chiba S, Kuwaki T, Miyagawa K, et al. Establishment and characterization of a unique human cell line that proliferates dependently on GM-CSF, IL-3, or erythropoietin. *J Cell Physiol*. 1989;140(2):323–34.
63. Vittori DC, Chamorro ME, Hernández YV, Maltaner RE, Nesse AB. Erythropoietin and derivatives: potential beneficial effects on the brain. *J Neurochem*. 2021;158(5):1032–57.
64. Al-Sarraf H, Malatiali S, Al-Awadi M, Redzic Z. Effects of erythropoietin on astrocytes and brain endothelial cells in primary culture during anoxia depend on simultaneous signaling by other cytokines and on duration of anoxia. *Neurochem Int*. 2018;113:34–45.
65. Minnerup J, Wersching H, Schäbitz WR. EPO for stroke therapy - Is there a future for further clinical development? *Exp Transl Stroke Med*. 2010;2(1):10.
66. Ostrowski D, Heinrich R. Alternative erythropoietin receptors in the nervous system. *J Clin Med*. 2018. <https://doi.org/10.3390/jcm7020024>.
67. Yao X, Wang D, Li H, Shen H, Shu Z, Chen G. Erythropoietin treatment in patients with acute ischemic stroke: a systematic review and meta-analysis of randomized controlled trials. *Curr Drug Deliv*. 2017;14(6):853–60.
68. Jelkmann W. Physiology and pharmacology of erythropoietin. *Transfus Med Hemother*. 2013;40(5):302–9.
69. Noguchi CT, Asavaritikrai P, Teng R, Jia Y. Role of erythropoietin in the brain. *Crit Rev Oncol Hematol*. 2007;64(2):159–71.
70. White UA, Coulter AA, Miles TK, Stephens JM. The STAT5A-mediated induction of pyruvate dehydrogenase kinase 4 expression by prolactin or growth hormone in adipocytes. *Diabetes*. 2007;56(6):1623–9.
71. Valle-Mendiola A, Soto-Cruz I. Energy metabolism in cancer: the roles of STAT3 and STAT5 in the regulation of metabolism-related genes. *Cancers*. 2020. <https://doi.org/10.3390/cancers12010124>.
72. Cadenas E, Davies KJ. Mitochondrial free radical generation, oxidative stress, and aging. *Free Radic Biol Med*. 2000;29(3–4):222–30.
73. Guo D, Wang Q, Li C, Wang Y, Chen X. VEGF stimulated the angiogenesis by promoting the mitochondrial functions. *Oncotarget*. 2017;8(44):77020–7.
74. Elias I, Franckhauser S, Bosch F. New insights into adipose tissue VEGF-A actions in the control of obesity and insulin resistance. *Adipocyte*. 2013;2(2):109–12.
75. Inoue M, Tsuji Y, Yoshimine C, Enomoto S, Morita Y, Osaki N, et al. Structural optimization of a TNFR1-selective antagonistic TNF $\alpha$  mutant to create new-modality TNF-regulating biologics. *J Biol Chem*. 2020;295(28):9379–91.
76. Mukandala G, Tynan R, Lanigan S, O'Connor JJ. The effects of hypoxia and inflammation on synaptic signaling in the CNS. *Brain Sci*. 2016. <https://doi.org/10.3390/brainsci6010006>.

## Publisher's Note

Springer Nature remains neutral with regard to jurisdictional claims in published maps and institutional affiliations.